Article

Cell Host & Microbe

Human-Specific Adaptations in Vpu Conferring Anti-tetherin Activity Are Critical for Efficient Early HIV-1 Replication *In Vivo*

Graphical Abstract

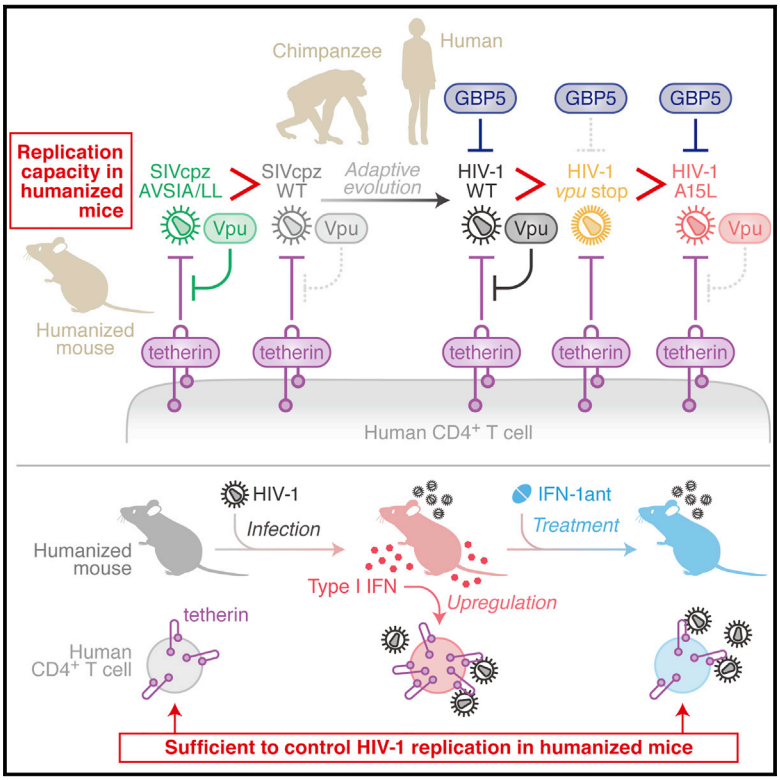

Highlights

- Vpu's anti-tetherin activity is critical for HIV-1 expansion during acute infection
- Vpu's anti-tetherin activity confers a selective advantage for HIV-1 spread *in vivo*
- Tetherin expression is upregulated upon HIV-1 infection in humanized mice
- Basal tetherin levels are sufficient to suppress HIV-1 replication independently of IFN-I

Authors

Eri Yamada, Shinji Nakaoka, Lukas Klein, ..., Yoshio Koyanagi, Daniel Sauter, Kei Sato

Correspondence

ksato@virus.kyoto-u.ac.jp

In Brief

The HIV-1-encoded accessory protein Vpu exerts several functions. Using a humanized mouse model and HIV-1 Vpu mutant viruses, Yamada et al. demonstrate that Vpu-mediated antagonism of the interferon-induced antiviral protein tetherin is critical for efficient viral spread during the initial phase of HIV-1 replication *in vivo*.

Yamada et al., 2018, Cell Host & Microbe *23*, 110–120
January 10, 2018
https://doi.org/10.1016/j.chom.2017.12.009

CellPress

CellPress

Cell Host & Microbe
Article

Human-Specific Adaptations in Vpu Conferring Anti-tetherin Activity Are Critical for Efficient Early HIV-1 Replication *In Vivo*

Eri Yamada,[1] Shinji Nakaoka,[2,3] Lukas Klein,[4] Elisabeth Reith,[4] Simon Langer,[4] Kristina Hopfensperger,[4] Shingo Iwami,[3,5,6] Gideon Schreiber,[7] Frank Kirchhoff,[4] Yoshio Koyanagi,[1] Daniel Sauter,[4] and Kei Sato[1,5,8,*]

[1]Laboratory of Systems Virology, Institute for Frontier Life and Medical Sciences, Kyoto University, Kyoto 6068507, Japan
[2]Institute of Industrial Sciences, The University of Tokyo, Tokyo 1538505, Japan
[3]PRESTO, Japan Science and Technology Agency, Saitama 3320012, Japan
[4]Institute of Molecular Virology, Ulm University Medical Center, Ulm 89081, Germany
[5]CREST, Japan Science and Technology Agency, Saitama 3220012, Japan
[6]Department of Biology, Faculty of Sciences, Kyushu University, Fukuoka 8128581, Japan
[7]Department of Biological Chemistry, Weizmann Institute of Science, Rehovot 76100, Israel
[8]Lead Contact
*Correspondence: ksato@virus.kyoto-u.ac.jp
https://doi.org/10.1016/j.chom.2017.12.009

SUMMARY

The HIV-1-encoded accessory protein Vpu exerts several immunomodulatory functions, including counteraction of the host restriction factor tetherin, downmodulation of CD4, and inhibition of NF-κB activity to facilitate HIV-1 infection. However, the relative contribution of individual Vpu functions to HIV-1 infection *in vivo* remained unclear. Here, we used a humanized mouse model and HIV-1 strains with selective mutations in *vpu* to demonstrate that the anti-tetherin activity of Vpu is a prerequisite for efficient viral spread during the early phase of infection. Mathematical modeling and gain-of-function mutations in SIVcpz, the simian precursor of pandemic HIV-1, corroborate this finding. Blockage of interferon signaling combined with transcriptome analyses revealed that basal tetherin levels are sufficient to control viral replication. These results establish tetherin as a key effector of the intrinsic immune defense against HIV-1, and they demonstrate that Vpu-mediated tetherin antagonism is critical for efficient viral spread during the initial phase of HIV-1 replication.

INTRODUCTION

Type I interferons (IFN-I) are key players of the innate antiviral immune response and efficiently suppress HIV-1 replication *in vitro* (Ho et al., 1985; Neil et al., 2007; Shirazi and Pitha, 1992). In part, this inhibitory effect is mediated by the induction of interferon-stimulated genes (ISGs) including cellular restriction factors such as TRIM5, APOBEC3, SAMHD1, and tetherin (reviewed in Doyle et al., 2015; Kluge et al., 2015). Additionally, IFN-inducible guanosine triphosphatases such as MX2 (Goujon et al., 2013; Kane et al., 2013) and GBP5 (Krapp et al., 2016) have recently been identified as HIV-1 inhibitors. To overcome the antiviral effects mediated by IFN-induced restriction factors, HIV-1 and related lentiviruses have evolved a variety of sophisticated antagonists (reviewed in Kirchhoff, 2010; Simon et al., 2015). For instance, the accessory viral protein U (Vpu) antagonizes tetherin (also known as BST2, CD317, and HM1.24) to enable efficient release of budding virions from infected cells (Neil et al., 2008; Van Damme et al., 2008).

In addition to counteracting tetherin, Vpu also downmodulates various immune receptors involved in innate and adaptive immunity, such as CD4, SLAM family member 6 (SLAMF6, also known as NTB-A), HLA-C, SLC38A1 (also known as SNAT1), and poliovirus receptor (PVR, also known as CD155) (Dubé et al., 2010; Matheson et al., 2015; Soper et al., 2017), and suppresses NF-κB-mediated immune activation (Galão et al., 2012; Sauter et al., 2015). While Vpu-mediated degradation of CD4, the primary receptor for HIV-1 infection, prevents superinfection and enables efficient release of fully infectious particles (Willey et al., 1992), downmodulation of HLA-C mediates evasion from cytotoxic T lymphocytes (Apps et al., 2016), and modulation of SLAMF6 (Shah et al., 2010) and PVR (Bolduan et al., 2014) might promote escape from natural killer cell-mediated cytolysis. In addition, the degradation of the alanine transporter SLC38A1 may help to prevent T cell activation (Sugden and Cohen, 2015).

Using hematopoietic stem cell (HSC)-transplanted humanized mice, we have shown that Vpu is crucial for efficient HIV-1 expansion during the acute phase of infection *in vivo* (Ikeda et al., 2016; Sato et al., 2012). However, it remained unclear which of the various Vpu functions is critical for this effect. Here, we characterized a series of HIV-1 strains including transmitted founder viruses containing selective or fully disruptive mutations in *vpu* and demonstrate that potent anti-tetherin activity is a prerequisite for efficient viral expansion during the initial phase of infection. While mutations selectively abrogating anti-tetherin activity of Vpu are deleterious, fully disrupted *vpu* genes may be tolerated in certain compartments, as they are associated with increased expression of the viral envelope protein

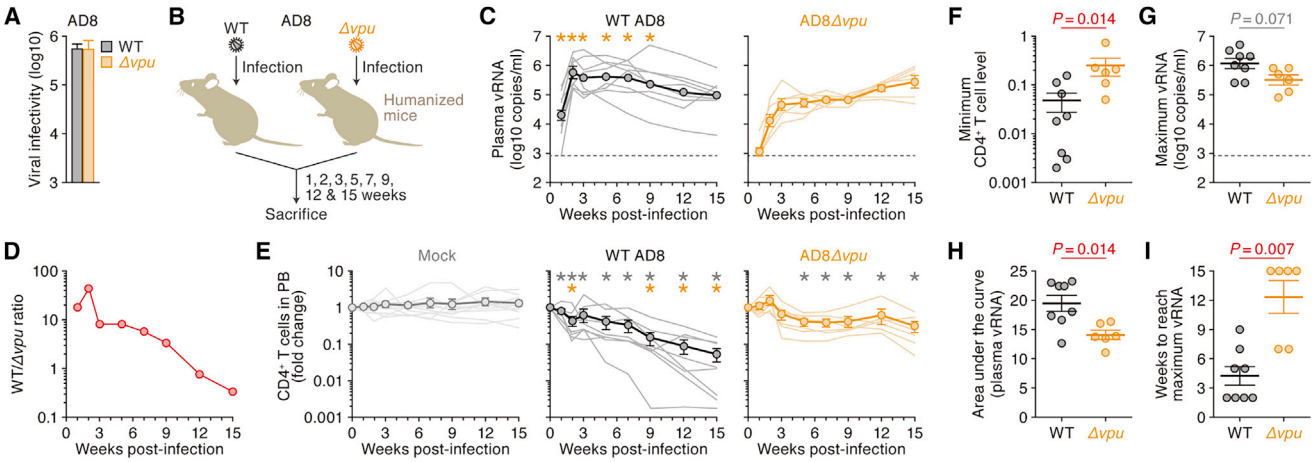

Figure 1. Dynamics of HIV-1 AD8 Replication in Humanized Mice

(A) Viral infectivity *in vitro*. HEK293T cells were transfected with the IMC of wild-type (WT) or *vpu*-deleted (Δ*vpu*) HIV-1 AD8, and infectious virus yield was determined by infection of TZM-bl reporter cells.

(B) Experimental setup. Humanized mice were inoculated with WT AD8 (n = 8), AD8Δ*vpu* (n = 6), or RPMI1640 (for mock infection, n = 10).

(C–E) The levels of plasma vRNA (C), ratio of vRNA levels in WT AD8 to AD8Δ*vpu* infected mice (D), and peripheral $CD4^+$ T cells ($CD45^+CD3^+CD4^+$ cells) (E) were determined for the indicated time points. In (C) and (E), circles indicate mean values ± SEM, and the pale lines indicate the results obtained from individual mice.

(F–I) Minimum $CD4^+$ T cell levels in PB (F), maximum vRNA (G), area under the curve of vRNA (H), and weeks to reach maximum vRNA (I) were analyzed. Mean values ± SEM are indicated by horizontal lines; circles represent values obtained from individual mice. Statistical difference was determined by Mann-Whitney U test. In (C) and (E), statistically significant differences ($P < 0.05$) versus mock and AD8Δ*vpu* are shown by grey and orange asterisks, respectively. NS, no statistical significance. The horizontal broken lines in (C) and (G) indicate the detection limit. See also Table S1.

(Env) and thus reduced sensitivity to GBP5 (Krapp et al., 2016) and/or other cellular proteins targeting Env. Furthermore, blockage of IFN-I signaling and transcriptome analyses in infected humanized mice revealed that basal tetherin levels are sufficient to restrict HIV-1 replication, although tetherin levels are further upregulated by IFN-I upon HIV-1 infection *in vivo*. Finally, we also monitored replication of an SIVcpz strain with adaptive mutations to human tetherin, reflecting the changes in the transmembrane domain of Vpu that occurred upon zoonotic transmission of SIVcpz to humans (Kirchhoff, 2010). Intriguingly, the gain-of-function mutant completely outcompeted its parental counterpart, which fails to antagonize human tetherin. Thus, our findings further support that the host restriction factor tetherin poses a significant barrier to successful zoonotic transmission of SIV to humans and highlight the *in vivo* selection advantage that pandemic HIV-1 strains gained by evolving Vpu-mediated anti-tetherin activity.

RESULTS

Vpu Promotes HIV-1 Expansion during the Acute Phase of Infection

To investigate the impact of Vpu on HIV-1 replication and $CD4^+$ T cell depletion *in vivo*, we infected humanized mice with the CCR5-tropic strain AD8 (± *vpu*) (Theodore et al., 1996). Equal infectious doses of the viral inocula were confirmed by infection of TZM-bl reporter cells (Figure 1A). To better reproduce the natural situation, mice were inoculated with a lower dose of viruses (1,500 infectious units per mouse) compared to our previous study (Sato et al., 2012). Eight mice were infected with wild-type (WT) AD8 and six with a *vpu*-deficient (Δ*vpu*) derivative (Figure 1B). During the first 9 weeks post-infection (wpi), the amount of viral RNA in the plasma of WT-AD8-infected mice was significantly higher than that of AD8Δ*vpu*-infected mice (Figure 1C). Notably, the ratio of WT to Δ*vpu* viral load (VL) decreased over the course of infection, demonstrating that *vpu* is particularly important during the acute phase (Figure 1D). We next analyzed the levels of $CD4^+$ T cells in peripheral blood (PB) and found that WT AD8 caused a more severe decline of peripheral $CD4^+$ T cells than AD8Δ*vpu* (Figure 1E). The minimum $CD4^+$ T cell level in WT-AD8-infected mice was about five times lower than that in AD8Δ*vpu*-infected mice (Figure 1F), indicating that AD8Δ*vpu* is less pathogenic than WT AD8. Although the maximum VL of WT AD8 was comparable to that of AD8Δ*vpu* ($P = 0.07$; Figure 1G), the area under the curve of the VL of WT AD8 was significantly higher than that of AD8Δ*vpu* ($P = 0.014$; Figure 1H). Moreover, WT AD8 and AD8Δ*vpu* reached their maximum VL, on average, at 4.3 wpi and 12.3 wpi, respectively (Figure 1I). Based on the experimental data shown in Figure 1, we also performed mathematical modeling and calculated the basic reproduction number R_0 as a metric of viral spread (Nowak and May, 2000). Mean R_0 values were 2.17 (95% CI: 1.47–3.16) and 1.65 (95% CI: 1.25–2.32) for WT AD8 and AD8Δ*vpu*, respectively (Table S1). Altogether, these findings are consistent with our previous data (Ikeda et al., 2016; Sato et al., 2012) and demonstrate that Vpu significantly enhances the efficacy of HIV-1 expansion during the acute phase of infection.

Anti-tetherin Activity of Vpu Is Critical for Efficient Viral Expansion during the Acute Phase of Infection

To assess the contribution of specific Vpu functions to this augmentation of viral replication *in vivo*, we generated two types of point mutants: one lacks anti-tetherin activity (A15L or A15L/A19L) (Kmiec et al., 2016; Vigan and Neil, 2010), while the other

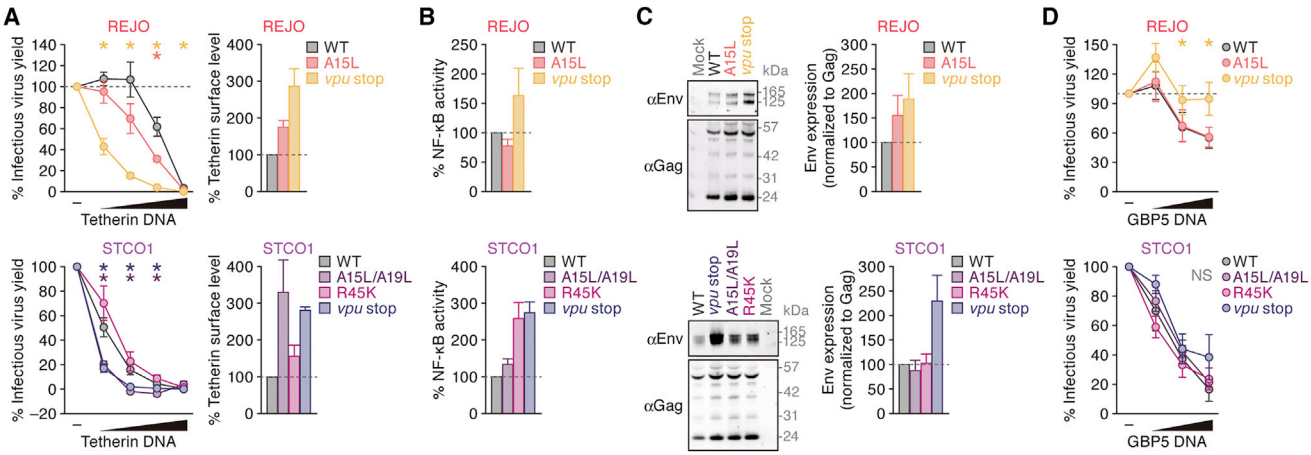

Figure 2. Characterization of HIV-1 REJO and STCO1 Mutants Thereof

(A) Counteraction of tetherin. On left, HEK293T cells were co-transfected with the indicated IMCs and increasing amounts of an expression plasmid for human tetherin. Two days post-transfection, cell culture supernatants were harvested, and infectious virus yield was determined by infection of TZM-bl reporter cells. On right, human PBMCs were transduced with the indicated VSV-G pseudotyped viruses. Three days post transduction, tetherin surface levels were quantified by flow cytometry. Infected cells were identified by intracellular p24 staining.

(B) Suppression of NF-κB activation. HEK293T cells were co-transfected with the indicated IMCs, an expression plasmid for constitutively active IKKβ, a reporter construct expressing firefly luciferase under the control of an NF-κB-dependent promoter, and a *Gaussia* luciferase vector for normalization. Two days post-transfection, a dual luciferase assay was performed, and firefly luciferase activity was normalized to *Gaussia* luciferase activity.

(C) Virion incorporation of Env. HEK293T cells were transfected with the indicated IMCs. Two days post-transfection, supernatants were harvested and analyzed by western blotting (left). Env levels were quantified and normalized to total Gag levels (right). The WT control was set to 100%.

(D) GBP5 sensitivity. HEK293T cells were co-transfected with increasing amounts of an expression construct for human GBP5 and the indicated IMCs. Supernatants were harvested two days post-transfection and used to infect TZM-bl reporter cells.

The mean values of three to seven independent experiments ± SEM are shown, and statistically significant differences ($P < 0.05$) versus WT are shown by asterisks. NS, no statistical significance. See also Figure S1.

one selectively fails to suppress NF-κB activation (R45K) (Sauter et al., 2015). Unfortunately, the generation of Vpu mutants selectively defective in CD4 downmodulation was not feasible, since changes in amino acid residues critical for CD4 degradation also impair other functions (Soper et al., 2017). As control, we included viruses with fully disrupted *vpu* genes (*vpu* stop) in our experiments. To mimic the *in vivo* situation, a transmitted founder virus (REJO) and a chronic control virus (STCO1) were used (Parrish et al., 2013). To verify selectivity of these mutants, we analyzed their ability to counteract tetherin (Figure 2A), to inhibit NF-κB activation (Figure 2B), and to decrease surface levels of CD4, HLA-C, SLAMF6, and PVR as well as total cellular levels of SLC38A1 (Figures S1A and S1B). As expected, the REJO A15L mutant lost activity against tetherin (Figure 2A) while maintaining its ability to inhibit NF-κB activation (Figure 2B) and to down-modulate CD4 and HLA-C (Figures S1A and S1B). In the case of STCO1, the A15L/A19L mutant fails to antagonize tetherin (Figure 2A), and the STCO1 R45K mutant specifically lost its ability to suppress NF-κB activation in both transfected HEK293T (Figure 2B) and infected $CD4^+$ T cells (Figure S1C). The importance of the R45 residue for suppressing NF-κB-dependent antiviral gene expression was confirmed by mRNA quantification of the NF-κB target *IFNB* (Figure S1D; Hotter et al., 2017). Notably, REJO and STCO1 Vpu had little if any effect on SLAMF6, PVR, and SLC38A1 (Figure S1B). As mutations in *vpu* might affect expression of Env, which is expressed from the same bicistronic mRNA (Schubert et al., 1999), we also determined virion infectivity and monitored Env levels by western blotting. Indeed, virion-associated Env levels and viral particle infectivity of REJO and STCO1 increased upon disruption of *vpu* (Figures 2C and S1E). In the presence of GBP5, the loss of a functional *vpu* gene might confer a selection advantage to the virus, since it is associated with increased Env levels (Krapp et al., 2016). In agreement with this hypothesis, REJO *vpu* stop was less sensitive to GBP5 than its WT and A15L counterparts (Figure 2D). In comparison, GBP5 suppressed STCO1 WT and its mutants to a similar extent (Figure 2D). Finally, WT REJO and its A15L mutant replicated with similar kinetics in a tetherin knockout (KO) Jurkat cell line expressing CCR5 (Figures S1F and S1G), indicating that the mutation in the transmembrane domain of Vpu has no tetherin-independent effects on viral replication.

To determine whether Vpu-mediated tetherin antagonism or NF-κB inhibition are associated with a selective advantage during acute HIV-1 infection, we performed *in vivo* competition assays (Nakano et al., 2017). Eight humanized mice were coinoculated with WT REJO and the A15L mutant, while nine mice were coinoculated with WT REJO and the respective *vpu* stop mutant (Figure 3A). In addition, seven mice were coinoculated with a mixture of WT STCO1 and its A15L/A19L, R45K, and *vpu* stop derivatives (Figure 3B). These mice were euthanized and sacrificed at 2 wpi, and the amount of viral RNA in plasma was assessed. In REJO-infected mice, both plasma VL (Figure 3A) and $CD4^+$ T cell decline (Figure S2A) were similar in the mice coinoculated with the A15L mutant and those with the *vpu* stop mutant. Additionally, plasma VL and the level of peripheral $CD4^+$ T cells were negatively correlated with statistical significance (Figure S2B; Spearman's

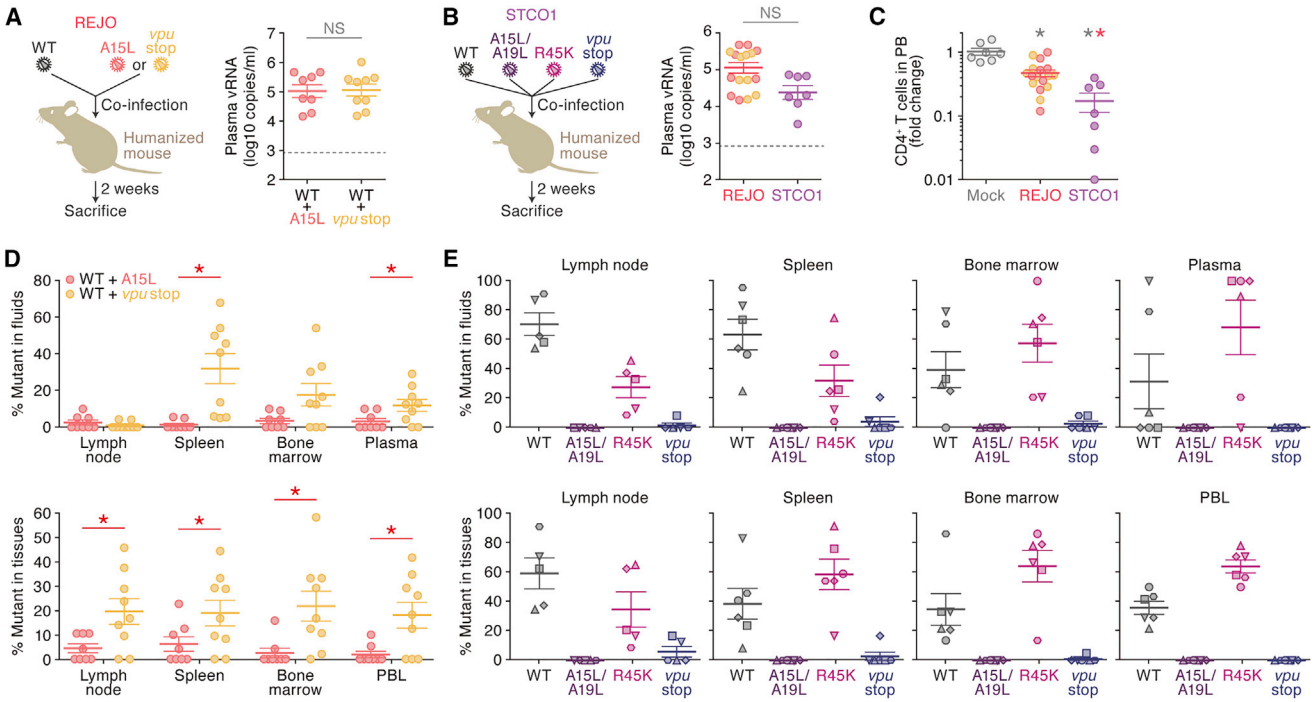

Figure 3. Dynamics of HIV-1 REJO and STCO1 Replication in Humanized Mice

(A and B) On the left, schemes of the *in vivo* competition assays. Humanized mice were coinoculated with WT REJO and either the A15L (n = 8) or *vpu* stop (n = 9) mutant thereof (A), or they were coinoculated with WT STCO1 and the A15L/A19L, R45K, and *vpu* stop derivatives thereof (n = 7) (B). On the right are plasma vRNA levels at 2 wpi. The horizontal broken line indicates the detection limit.

(C) Fold change of the level of peripheral $CD4^+$ T cells ($CD45^+CD3^+CD4^+$ cells) analyzed at 2 wpi.

(D and E) Percentage of mutant viruses (A15L or *vpu* stop in D or WT, A15L/A19L, R45K, or *vpu* stop in E) in fluids (top) and tissues (bottom). In (E), each symbol represents an individual mouse.

The mean values ± SEM are indicated by horizontal lines; circles represent values obtained for individual mice. In (C), statistically significant differences ($P < 0.05$) versus mock and REJO are shown by grey and red asterisks, respectively. In (D), statistically significant differences ($P < 0.05$) are shown by red asterisks. NS, no statistical significance. See also Figure S2.

$r = -0.699$, $P = 0.0052$ by Spearman's rank correlation coefficient). Although the plasma VL in STCO1-infected mice was not significantly lower than that in REJO-infected mice ($P = 0.062$; Figure 3B), $CD4^+$ T cell levels in PB decreased even more ($P = 0.0018$; Figure 3C).

We next investigated viral expansion in various tissues (cell-associated virus) and the respective fluids (cell-free virus). Significantly higher levels of cell-associated and cell-free viral RNA (vRNA) were found in the lymphoid tissues such as spleen and bone marrow than in the periphery (peripheral blood leukocyte, or PBL, and plasma) of both REJO- (Figure S2C) and STCO1-infected mice (Figure S2D). In REJO-infected mice, the levels of cell-free vRNA in the tissue fluids of the mice coinoculated with the *vpu* stop mutant were comparable to those coinfected with the A15L mutant (Figure S2E, top). In contrast, the levels of cell-associated vRNA in the mesenteric lymph nodes, spleen, and bone marrow of mice coinoculated with the *vpu* stop mutant were significantly higher than those obtained with the A15L mutant (Figure S2E, bottom). Furthermore, we sequenced the complete *vpu* open reading frame to determine the frequency of each derivative in the respective tissues and fluids. Notably, we never observed mutations or recombination events in *vpu*. Since reversion of the mutant viruses to WT may have been masked by our coinfection setup, four humanized mice were infected solely with the REJO A15L mutant. However, even at 9 wpi, this A15L mutation was maintained in the plasma of these mice, suggesting that reversion does not frequently occur in this experimental system.

In almost all cases, the REJO WT virus dominated over the A15L and *vpu* stop mutants (Figure 3D). Notably, however, the REJO *vpu* stop mutant was also readily detectable, and its percentage in the cell-associated vRNA was significantly higher than that of the A15L mutant, which was hardly detected in any of the samples (Figure 3D, bottom). Furthermore, the proportions of the REJO *vpu* stop mutant in splenic fluid and plasma were significantly higher than those of the A15L mutant (Figure 3D, top). These results suggest that REJO *vpu* stop replicates more efficiently in lymphoid tissues than REJO A15L, which specifically fails to antagonize tetherin. In STCO1-infected mice, the majority of vRNA detected in tissues and fluids represented WT and R45K mutants, while both the A15L/A19L and *vpu* stop mutants were hardly detectable (Figure 3E). In summary, these findings show that the anti-tetherin activity of Vpu is essential for efficient viral replication during the initial phase of infection, while its ability to suppress NF-κB activation is dispensable during the early stage in this *in vivo* model.

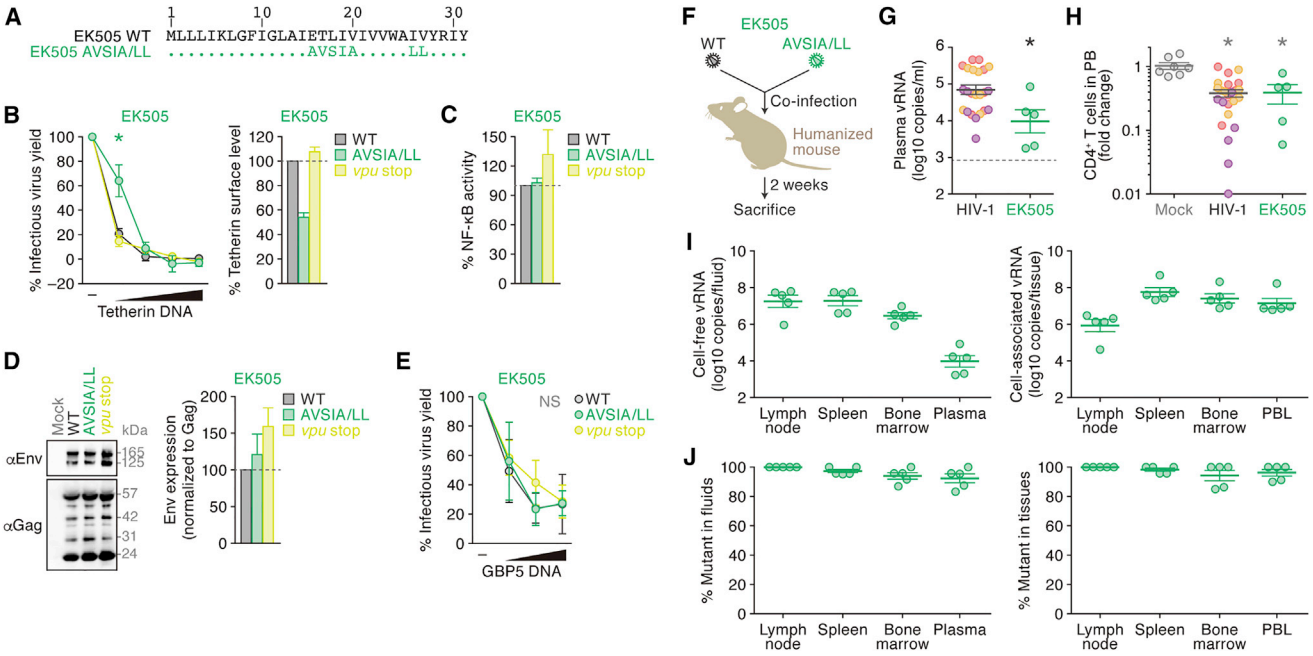

Figure 4. Dynamics of SIVcpz EK505 Replication in Humanized Mice

(A) Amino acid sequence of the N-terminus of EK505 WT Vpu and its AVSIA/LL mutant.

(B–E) Counteraction of tetherin (B), suppression of NF-κB activation (C), incorporation of Env in virion (D), and GBP5 sensitivity (E). Experiments were performed as described for Figure 2.

(F) Scheme of the *in vivo* competition assay. Five humanized mice were coinoculated with WT EK505 and its AVSIA/LL mutant.

(G and H) The levels of plasma vRNA (G) and fold change of the level of peripheral CD4$^+$ T cells (H) were analyzed at 2 wpi. The horizontal broken line in (G) indicates the detection limit.

(I) Levels of cell-associated vRNA in fluids (left) and tissues (right).

(J) Percentage of the EK505 AVSIA/LL mutant in fluids (left) and tissues (right). In (B) through (E), the mean values of three to six independent experiments ± SEM are shown, and statistically significant difference ($P < 0.05$) versus WT is shown by asterisk. In (G) through (J), the mean values ± SEM are indicated by horizontal lines; circles represent values obtained for individual mice. In (G) and (H), statistically significant differences ($P < 0.05$) versus mock and HIV-1 are shown by grey and black asterisks, respectively. NS, no statistical significance. See also Figure S3.

Acquisition of Anti-tetherin Activity by SIVcpz Vpu Confers a Selective Advantage for Viral Spread *In Vivo*

To further investigate the importance of Vpu's ability to antagonize tetherin, we conducted gain-of-function experiments using SIVcpz, the simian precursor of HIV-1, whose Vpu is unable to counteract human tetherin (Kluge et al., 2013; Sauter et al., 2009). We had previously identified mutations in the transmembrane domain of SIVcpz Vpu that confer the ability to counteract human tetherin (Kluge et al., 2013; Sauter et al., 2012), and we inserted these mutations (designated AVSIA/LL) (Figure 4A) into an infectious molecular clone (IMC) of SIVcpz strain EK505. Notably, the AVSIA/LL mutant gained the ability to enhance virus release by antagonizing human tetherin (Figure 4B, left) and significantly downregulated tetherin from the surface of infected cells (Figure 4B, right). While this mutation did not significantly affect NF-κB suppression (Figure 4C), Env incorporation (Figure 4D), virion infectivity (Figure S3A), sensitivity to GBP5 (Figure 4E), or downmodulation of CD4 (Figure S3B), it abrogated the ability of Vpu to decrease surface HLA-C levels (Figure S3C). SIVcpz EK505 has previously been shown to replicate in both human and chimpanzee cells (Bibollet-Ruche et al., 2012). The replication kinetics of WT EK505 was similar to that of the *vpu*-deficient mutant, while the AVSIA/LL mutation significantly decreased the replicative fitness in tetherin KO Jurkat cells (Figure S4D).

To determine the impact of this gain of anti-tetherin activity on viral replication *in vivo*, five humanized mice were coinoculated with WT EK505 and the AVSIA/LL mutant (Figure 4F). As shown in Figure 4G, all five mice exhibited viremia, but the plasma VL of EK505-infected mice was significantly lower than that of the mice infected with HIV-1 ($P = 0.028$; versus HIV-1 REJO and STCO1). Nevertheless, a significant decline of peripheral CD4$^+$ T cells was detected in EK505-infected mice ($P = 0.010$; Figure 4H). SIVcpz EK505 replicated systemically in humanized mice (Figure 4I), and intriguingly, the AVSIA/LL derivative was predominant in all lymphoid tissues and fluids assessed (Figure 4J). These results further highlight the importance of tetherin counteraction for the establishment of systemic viral infection.

Tetherin Expression Is Upregulated upon HIV-1 Infection in Humanized Mice

To address whether HIV-1 infection elicits IFN-I responses in humanized mice during the initial phase of infection, splenic human CD4$^+$ T cells were sorted and global transcriptome analyses were performed. As summarized in Figures 5A and 5B, the expression levels of 631 genes in splenic human CD4$^+$ T cells of HIV-1-infected mice were significantly changed compared to those of uninfected mice (listed in Table S2). Gene ontology

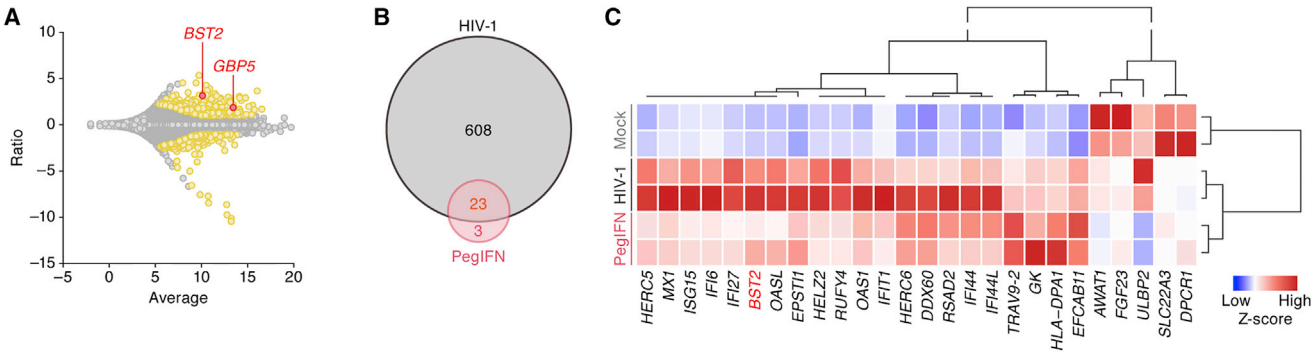

Figure 5. Transcriptome Analysis on CD4$^+$ Cells of Infected Humanized Mice

(A) An MA plot of the datasets from CD4$^+$ cells (CD45$^+$CD3$^+$CD8$^-$ cells) of HIV-1-infected mice. The average (x axis) and the ratio of normalized gene expression (HIV-infected to mock-infected) (y axis) are shown. Each dot indicates a gene, and the genes selected as differentially expressed (FDR < 0.05) and upregulated or downregulated more than 2-fold (compared to mock-infected mice) are shown in yellow. *BST2* and *GBP5* are highlighted in red.

(B) Venn diagram of differentially expressed genes (DEGs) in HIV-1-infected (n = 631) and pegIFN-treated mice (n = 26). The criteria for DEG selection are described in the Supplemental Information.

(C) Heatmap with hierarchical clustering of selected DEGs from mock-infected, HIV-1-infected and pegIFN-treated mice. See also Figure S4 and Tables S2, S3, S4, and S5.

analyses revealed that HIV-1 infection induced IFN-α, IFN-β and IFN-γ responses (Table S3). As control, we treated two humanized mice with pegylated IFN-α (pegIFN) and sacrificed them at 1 week post-treatment. Flow cytometry demonstrated that expression levels of tetherin (Figure S4A) and ISG15 (Figure S4B) were increased in pegIFN-treated humanized mice. Furthermore, transcriptome analysis revealed that the mRNA expression levels of 26 genes were significantly modulated by pegIFN treatment (listed in Tables S4 and S5) and that 23 of them were also differentially expressed upon HIV-1 infection (Figure 5B). Notably, the mRNA level of *BST2* (encoding tetherin) was increased by both HIV-1 infection and pegIFN treatment (Figures 5A and 5C). In contrast, the mRNA expression of *GBP5* was upregulated in HIV-1-infected mice (Figure 5A), but not induced by pegIFN treatment (Tables S2 and S4). The induction of only 26 genes upon pegIFN may seem low, but previous data suggest that the expression of most genes induced by IFN-α may already have decreased to normal levels by 7 days post-stimulation (Bolen et al., 2014; Jilg et al., 2014). In agreement with this possibility, the expression levels of *BST2* and *IFI44L* reach their maxima at 0.5–1 day post treatment and start decreasing again thereafter (Figure S4C).

Tetherin Suppresses Viral Replication during Acute Infection Independently of IFN-I Signaling

Based on the transcriptome analyses (Figure 5), we hypothesized that induction of tetherin expression by IFN-I may be required for restriction of retroviral replication. To test this, five humanized mice were coinoculated with both WT REJO and the A15L mutant lacking anti-tetherin activity and subsequently treated with an antagonist for human IFN-I (IFN-1ant) (Levin et al., 2014; Sandler et al., 2014; Figure 6A). Surprisingly, IFN-1ant treatment neither affected the plasma VL (Figure 6B) nor CD4$^+$ T cell decline at 2 wpi (Figure 6C). To verify the effect of IFN-1ant treatment, the mRNA expression levels of five ISGs were analyzed by real-time RT-PCR. HIV-1 infection significantly enhanced ISG expression in splenic CD4$^+$ T cells, while this upregulation was significantly suppressed by IFN-1ant treatment (Figure 6D). Flow cytometric analyses also revealed that HIV-1 infection significantly induced tetherin expression on splenic CD4$^+$ T cells, while tetherin expression levels on splenic CD4$^+$ T cells of infected mice receiving IFN-1ant treatment were similar to those of uninfected mice (Figure 6E). The induction of tetherin expression by HIV-1 infection and its blockage by IFN-1-ant treatment was confirmed in splenic CD45$^+$ leukocytes (Figure S5A), and HIV-1-induced ISG15 expression was suppressed by IFN-1ant (Figure S5B). Thus, IFN-1ant treatment did not affect plasma VL, although it efficiently suppressed the induction of IFN-I signaling by HIV-1 infection in humanized mice. Furthermore, flow cytometric analyses revealed that IFN-1ant treatment did not affect the percentage of HIV-1-infected cells in spleen (Figure 6F). We then assessed the amount of vRNA copies and sequenced the *vpu*-coding region in tissues and fluids of infected mice treated with IFN-1ant. Whereas IFN-1ant treatment did not affect the levels of cell-associated vRNA, the quantities of cell-free vRNA in the fluids of lymph node and spleen of IFN-1-ant-treated mice were 58-fold (P = 0.0034) and 42-fold (P = 0.013) higher than those of untreated mice, respectively (Figure 6G). Although the percentage of the A15L mutant in the lymph nodes of IFN-1ant-treated mice was higher than that of untreated mice, those in the other tissues and fluids tested were not affected by IFN-1ant treatment (Figure 6H). Thus, basal tetherin expression is sufficient to exert a significant antiviral effect *in vivo.*

DISCUSSION

In the present study, we show that the multifunctional accessory protein Vpu enables efficient spread of HIV-1 during acute infection by counteracting the host restriction factor tetherin. Competition assays of primary HIV-1 strains and derivatives thereof lacking specific Vpu functions revealed that the anti-tetherin activity of Vpu is more important for early replication in humanized mice than its ability to suppress NF-κB activation. In agreement

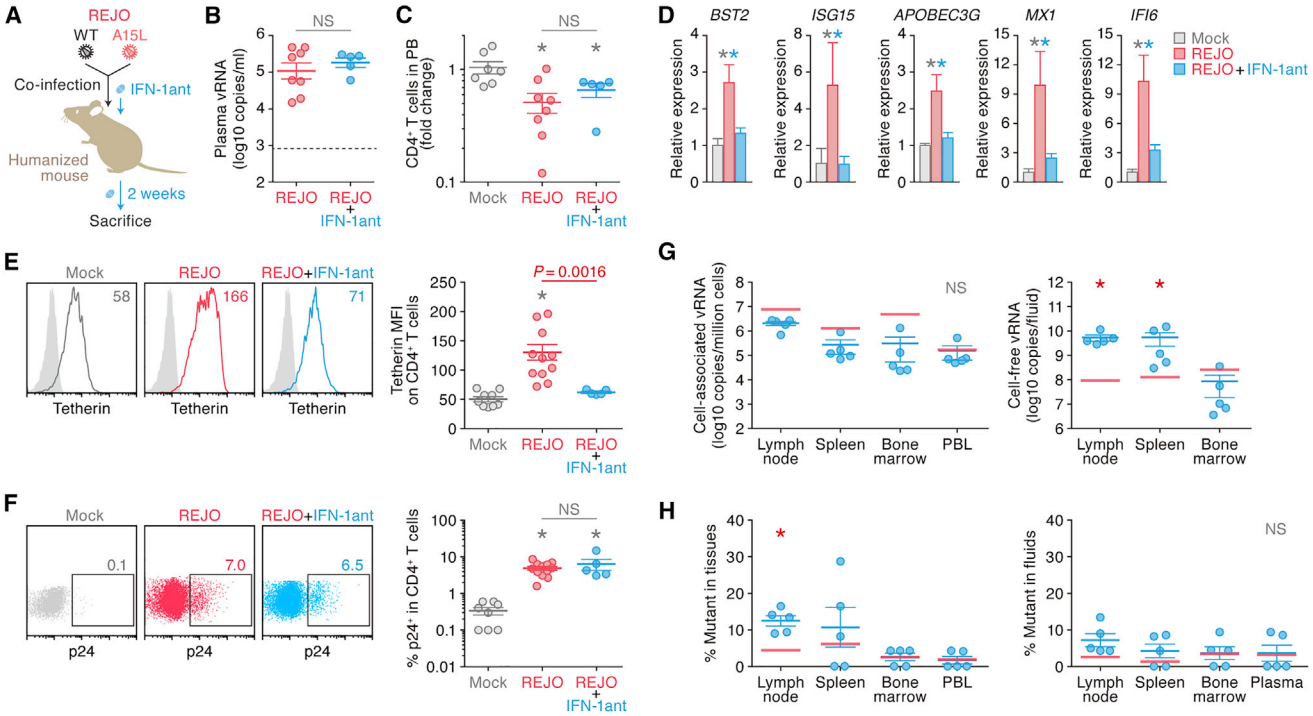

Figure 6. Effect of IFN-I Blockage on HIV-1 REJO Replication in Humanized Mice

(A) Scheme of the *in vivo* competition assay. Five humanized mice were coinoculated with WT REJO and its A15L mutant. These mice were treated daily with IFN-1ant (2 μg per mouse, intramuscular injection).

(B and C) The levels of plasma vRNA (B) and peripheral $CD4^+$ T cells ($CD45^+CD3^+CD4^+$ cells) (C) were analyzed at 2 wpi. The horizontal broken line in (B) indicates the detection limit.

(D) mRNA expression levels of five ISGs (*BST2, ISG15, APOBEC3G, MX1*, and *IFI6*) were analyzed by real-time RT-PCR.

(E and F) Surface levels of tetherin (E) and the percentage of $p24^+$ cells in splenic $CD4^+$ T cells ($CD45^+CD3^+CD8^-$ cells) (F) were analyzed by flow cytometry. Representative plots (left) and a summary of all results (right) are shown. The numbers in the plots indicate MFI (E) and percentage (F), respectively. In (E), the filled grey histogram indicates isotype control.

(G) Levels of cell-associated vRNA in tissues (left) and cell-free vRNA in fluids (right).

(H) Percentage of the REJO A15L derivative in tissues (left) and fluids (right). In (G) and (H), red horizontal lines indicate the results obtained in the absence of IFN-1ant treatment (n = 8).

Mean values ± SEM obtained from IFN-1ant-treated mice are indicated by blue horizontal lines; circles represent values obtained for individual mice. Statistically significant differences ($P < 0.05$, determined by Mann-Whitney U test) are indicated by asterisks. Grey (C–F), blue (D), and red (G and H) asterisks indicate differences versus mock, REJO with IFN-1ant, and REJO without IFN-1ant, respectively. NS, no statistical significance. See also Figure S5.

with this, a mutant of SIVcpz EK505 capable of counteracting human tetherin outcompeted the respective WT virus. Notably, this mutant mimics gain-of-function changes in Vpu that preceded the emergence of pandemic HIV-1. Thus, our findings corroborate the hypothesis that the acquisition of potent Vpu-mediated anti-tetherin activity facilitated the successful zoonotic transmission of SIVcpz and its subsequent spread in the human population.

Transcriptome and flow cytometry analyses revealed that HIV-1 infection markedly upregulated the expression of tetherin in an IFN-I-dependent manner. Notably, however, blockage of IFN-I signaling did not affect the replication efficacy of viruses failing to antagonize tetherin. Thus, our findings not only demonstrate that Vpu-mediated tetherin antagonism promotes efficient HIV-1 replication during the acute phase of infection but also show that basal tetherin levels are sufficient to restrict viral replication *in vivo*.

Intriguingly, a *vpu* stop mutant of HIV-1 REJO replicated and spread more efficiently than the A15L mutant, although the latter retained its ability to suppress NF-κB activation and to downmodulate CD4 and HLA-C. This observation supports the idea of a trade-off mechanism in which loss of Vpu is partly compensated for by increased Env expression, resulting in higher virion infectivity and reduced sensitivity towards restriction factors targeting the viral envelope protein (Krapp et al., 2016). In agreement with this, REJO *vpu* stop viruses were significantly less sensitive against GBP5 than the respective A15L mutant. Notably, HIV-1 STCO1 did not gain significant resistance against GBP5 upon disruption of *vpu*, which may explain why it almost completely failed to replicate in humanized mice. This finding also suggests that lack of *vpu* expression does not always coincide with reduced sensitivity to GBP5. While the determinants of GBP5-mediated restriction are not fully understood, it has been shown that even WT viruses differ considerably in their sensitivity to GBP5 (Krapp et al., 2016). For example, WT REJO is less sensitive to GBP5 than WT STCO1 or EK505, (Figures 2D and 4E) and the observed increase in Env expression may not be sufficient to overcome the intrinsically high susceptibility of the latter two

viruses. In agreement with previous observations in infected patients (Bartha et al., 2014), we found that *GBP5* expression is upregulated in HIV-1-infected mice. Taken together, these observations support a significant role of GBP5 and/or other cellular factors targeting viral infectivity and may explain the emergence of *vpu*-deficient viruses in some HIV-1-infected individuals (Krapp et al., 2016; Schubert et al., 1999). Notably, different compartments may select for HIV-1 variants with different amounts of virion-associated Env: in PB, low levels of Env may be advantageous due to reduced antibody neutralization and antibody-mediated cellular cytotoxcity (Klein and Bjorkman, 2010). In contrast, higher Env levels may be tolerated in immunosecluded compartments such as the brain. In agreement with this, inactivating *vpu* mutations are commonly found in brain-derived HIV-1 strains (Krapp et al., 2016; Li et al., 1991). Intriguingly, two previous studies also reported the emergence of *vpu*-deficient mutants during *in vitro* HIV-1 passage that were characterized by increased replicative fitness and enhanced cell-to-cell spread (Gummuluru et al., 2000; Hamm et al., 1999). These findings further support that the loss of a functional *vpu* gene can be associated with a selection advantage under certain environmental conditions. Notably, however, Gummuluru et al. (2000) demonstrated that enhanced cell-to-cell spread of their *vpu*-deficient HIV-1 variant was not due to increased Env expression. Thus, Env-dependent and -independent phenotypic features of *vpu*-deficient viruses may compensate for the loss of efficient tetherin counteraction.

While HIV-1 exploits NF-κB to initiate viral gene expression, this transcription factor also plays a pivotal role in antiviral immune responses (Chan and Greene, 2012). Here, we demonstrate that the R45K mutant of HIV-1 STCO1, which specifically lost its ability to suppress NF-κB activation, spreads as efficiently in humanized mice as the parental WT virus. These findings suggest that Vpu's ability to inhibit NF-κB signaling is dispensable for viral spread during the initial phase of infection. However, we cannot exclude a crucial role of Vpu-mediated NF-κB inhibition during the chronic phase of infection. Furthermore, the importance of this activity may be underestimated in our experimental setup, as HSC-transplanted humanized mice harbor little if any functional acquired immunity (Shultz et al., 2012; Yamada et al., 2015). Thus, Vpu functions such as HLA-C downmodulation or NF-κB inhibition may well be more important during later stages of HIV-1 infection in infected human individuals.

Certain ISGs exert significant antiviral activity only upon induction by IFNs. One recently described example is TRIM56, which potently suppresses retroviral replication in response to IFN but fails to restrict HIV-1 at basal expression levels (Kane et al., 2016). In comparison, our findings suggest that basal level of tetherin expression is sufficient to control HIV-1 replication during acute infection *in vivo*. Intriguingly, Liberatore and Bieniasz previously demonstrated that induction of tetherin expression by IFN-I signaling is required to reveal its activity against murine retroviruses (Liberatore and Bieniasz, 2011). These findings suggest that HIV-1 may be more sensitive to tetherin than murine retroviruses, and they might explain its dependency on an efficient tetherin antagonist to efficiently spread in humans. In agreement with this, basal expression levels of tetherin are not only detectable in $CD4^+$ T cells of humanized mice (Dave et al., 2013; Sato et al., 2012) but also in those of HIV-negative human individuals (Homann et al., 2011).

In summary, we show that tetherin is an efficient and early effector of the intrinsic immune response and provide evidence that its basal expression levels can be sufficient to restrict replication and dissemination of HIV-1 *in vivo*. Furthermore, the promotion of early viral replication by Vpu could be ascribed to its ability to counteract tetherin. As most primate lentiviruses fail to antagonize the human tetherin ortholog, our findings also demonstrate that the evolution of an efficient tetherin antagonist facilitates their successful zoonotic transmission to humans. While mutations selectively abrogating the anti-tetherin activity of Vpu are detrimental for viral replication, a complete loss of *vpu* can be tolerated in some cases, since it may be associated with increased virion infectivity and/or reduced sensitivity towards anti-retroviral factors targeting Env.

STAR★METHODS

Detailed methods are provided in the online version of this paper and include the following:

- KEY RESOURCES TABLE
- CONTACT FOR REAGENT AND RESOURCE SHARING
- EXPERIMENTAL MODEL AND SUBJECT DETAILS
  - Ethics Statement
  - Humanized Mice
  - Cells and Viruses
- METHOD DETAILS
  - Expression Plasmids
  - Western Blotting
  - TZM-bl Reporter Assay and Virion Infectivity
  - NF-κB Reporter Assay
  - Generation of Tetherin KO Jurkat Cells by Using CRISPR-Cas9 System
  - Infection of Humanized Mice and *In Vivo* Competition Assay
  - Infection of Primary Cells *Ex Vivo*
  - RNA Extraction, RT-PCR, TOPO Cloning and Sanger Sequencing
  - Quantitative RT-PCR
  - Flow Cytometry, Hematometry, and Cell Sorting
  - Global Transcriptome Analysis
  - Treatment with PegIFN and IFN-1ant
  - Mathematical Modeling
- QUANTIFICATION AND STATISTICAL ANALYSIS
- DATA AND SOFTWARE AVAILABILITY

SUPPLEMENTAL INFORMATION

Supplemental Information includes five figures and six tables and can be found with this article online at https://doi.org/10.1016/j.chom.2017.12.009.

ACKNOWLEDGMENTS

We would like to thank the UCLA CFAR Gene and Cellular Therapy Core Facility for providing human HSCs (UCLA Center for AIDS Research NIH/NIAID 5P30 AI028697). We also thank Junko S. Takeuchi (National Institute for Infectious Diseases, Japan), Beatrice H. Hahn (University of Pennsylvania, USA), Dong Sung An (University of California, Los Angeles, USA), Bernd Baumann (Ulm University, Germany), Barton F. Haynes and Hua-Xin Liao (Duke

University School of Medicine, USA), and Klaus Strebel (National Institute of Health, USA) for providing materials. This study was supported in part by AMED J-PRIDE 17fm0208006h0001 (to K.S.); JST CREST (to K.S. and S.I.); JSPS KAKENHI Grants-in-Aid for Scientific Research C 15K07166 (to K.S.); Scientific Research B (Generative Research Fields) 16KT0111 (to K.S. and S.I.); Scientific Research on Innovative Areas 16H06429 (to K.S. and S.I.), 16K21723 (to K.S. and S.I.), and 17H05813 (to K.S.); Takeda Science Foundation (to K.S.); Salt Science Research Foundation (to K.S.); Smoking Research Foundation (to K.S.); Chube Ito Foundation (to K.S.); Fordays Self-Reliance Support in Japan (to K.S.); Mishima Kaiun Memorial Foundation (to K.S.); Tobemaki Foundation (to K.S.); JSPS Core-to-Core program, A. Advanced Research Networks (to F.K., Y.K., and D.S.); AMED Research on HIV/AIDS 16fk0410203h002 (to Y.K.); JST PRESTO (to S.N. and S.I.); Priority Programme 1923 of the German Research Foundation (to D.S. and F.K.); Junior Professorship Programme of the state of Baden-Wuerttemberg (to D.S.); International Graduate School in Molecular Medicine Ulm (to S.L., E.R., and K.H.); and an ERC Advanced grant (to F.K.).

AUTHOR CONTRIBUTIONS

E.Y., L.K., E.R., S.L., K.H., and D.S. performed the experiments and analyzed the data. S.N. and S.I. conducted mathematical and transcriptome analyses. G.S., F.K., and Y.K. provided reagents. D.S. and K.S. conceived and designed the experiments. E.Y., F.K., Y.K., D.S., and K.S. wrote the manuscript.

Received: April 11, 2017
Revised: September 11, 2017
Accepted: December 1, 2017
Published: January 10, 2018

REFERENCES

Apps, R., Del Prete, G.Q., Chatterjee, P., Lara, A., Brumme, Z.L., Brockman, M.A., Neil, S., Pickering, S., Schneider, D.K., Piechocka-Trocha, A., et al. (2016). HIV-1 Vpu mediates HLA-C downregulation. Cell Host Microbe *19*, 686–695.

Bartha, I., McLaren, P.J., Ciuffi, A., Fellay, J., and Telenti, A. (2014). GuavaH: a compendium of host genomic data in HIV biology and disease. Retrovirology *11*, 6.

Benjamini, Y., and Hochberg, Y. (1995). Controlling the false discovery rate: a practical and powerful approach to multiple testing. J. R. Stat. Soc. Series B Stat. Methodol. *57*, 289–300.

Bibollet-Ruche, F., Heigele, A., Keele, B.F., Easlick, J.L., Decker, J.M., Takehisa, J., Learn, G., Sharp, P.M., Hahn, B.H., and Kirchhoff, F. (2012). Efficient SIVcpz replication in human lymphoid tissue requires viral matrix protein adaptation. J. Clin. Invest. *122*, 1644–1652.

Bolduan, S., Reif, T., Schindler, M., and Schubert, U. (2014). HIV-1 Vpu mediated downregulation of CD155 requires alanine residues 10, 14 and 18 of the transmembrane domain. Virology *464-465*, 375–384.

Bolen, C.R., Ding, S., Robek, M.D., and Kleinstein, S.H. (2014). Dynamic expression profiling of type I and type III interferon-stimulated hepatocytes reveals a stable hierarchy of gene expression. Hepatology *59*, 1262–1272.

Chan, J.K., and Greene, W.C. (2012). Dynamic roles for NF-κB in HTLV-I and HIV-1 retroviral pathogenesis. Immunol. Rev. *246*, 286–310.

Dave, V.P., Hajjar, F., Dieng, M.M., Haddad, É., and Cohen, E.A. (2013). Efficient BST2 antagonism by Vpu is critical for early HIV-1 dissemination in humanized mice. Retrovirology *10*, 128.

Doyle, T., Goujon, C., and Malim, M.H. (2015). HIV-1 and interferons: who's interfering with whom? Nat. Rev. Microbiol. *13*, 403–413.

Dubé, M., Bego, M.G., Paquay, C., and Cohen, E.A. (2010). Modulation of HIV-1-host interaction: role of the Vpu accessory protein. Retrovirology *7*, 114.

Ebina, H., Misawa, N., Kanemura, Y., and Koyanagi, Y. (2013). Harnessing the CRISPR/Cas9 system to disrupt latent HIV-1 provirus. Sci. Rep. *3*, 2510.

Eisen, M.B., Spellman, P.T., Brown, P.O., and Botstein, D. (1998). Cluster analysis and display of genome-wide expression patterns. Proc. Natl. Acad. Sci. USA *95*, 14863–14868.

Fouchier, R.A., Meyer, B.E., Simon, J.H., Fischer, U., and Malim, M.H. (1997). HIV-1 infection of non-dividing cells: evidence that the amino-terminal basic region of the viral matrix protein is important for Gag processing but not for post-entry nuclear import. EMBO J. *16*, 4531–4539.

Galão, R.P., Le Tortorec, A., Pickering, S., Kueck, T., and Neil, S.J. (2012). Innate sensing of HIV-1 assembly by Tetherin induces NFκB-dependent proinflammatory responses. Cell Host Microbe *12*, 633–644.

Goujon, C., Moncorgé, O., Bauby, H., Doyle, T., Ward, C.C., Schaller, T., Hué, S., Barclay, W.S., Schulz, R., and Malim, M.H. (2013). Human MX2 is an interferon-induced post-entry inhibitor of HIV-1 infection. Nature *502*, 559–562.

Gummuluru, S., Kinsey, C.M., and Emerman, M. (2000). An *in vitro* rapid-turnover assay for human immunodeficiency virus type 1 replication selects for cell-to-cell spread of virus. J. Virol. *74*, 10882–10891.

Hamm, T.E., Rekosh, D., and Hammarskjöld, M.L. (1999). Selection and characterization of human immunodeficiency virus type 1 mutants that are resistant to inhibition by the transdominant negative RevM10 protein. J. Virol. *73*, 5741–5747.

Ho, D.D., Hartshorn, K.L., Rota, T.R., Andrews, C.A., Kaplan, J.C., Schooley, R.T., and Hirsch, M.S. (1985). Recombinant human interferon alfa-A suppresses HTLV-III replication in vitro. Lancet *1*, 602–604.

Homann, S., Smith, D., Little, S., Richman, D., and Guatelli, J. (2011). Upregulation of BST-2/Tetherin by HIV infection *in vivo*. J. Virol. *85*, 10659–10668.

Hotter, D., Kirchhoff, F., and Sauter, D. (2013). HIV-1 Vpu does not degrade interferon regulatory factor 3. J. Virol. *87*, 7160–7165.

Hotter, D., Krabbe, T., Reith, E., Gawanbacht, A., Rahm, N., Ayouba, A., Van Driessche, B., Van Lint, C., Peeters, M., Kirchhoff, F., and Sauter, D. (2017). Primate lentiviruses use at least three alternative strategies to suppress NF-κB-mediated immune activation. PLoS Pathog. *13*, e1006598.

Ikeda, H., Nakaoka, S., de Boer, R.J., Morita, S., Misawa, N., Koyanagi, Y., Aihara, K., Sato, K., and Iwami, S. (2016). Quantifying the effect of Vpu on the promotion of HIV-1 replication in the humanized mouse model. Retrovirology *13*, 23.

Ito, M., Hiramatsu, H., Kobayashi, K., Suzue, K., Kawahata, M., Hioki, K., Ueyama, Y., Koyanagi, Y., Sugamura, K., Tsuji, K., et al. (2002). NOD/SCID/$\gamma_{(c)}^{null}$ mouse: an excellent recipient mouse model for engraftment of human cells. Blood *100*, 3175–3182.

Jilg, N., Lin, W., Hong, J., Schaefer, E.A., Wolski, D., Meixong, J., Goto, K., Brisac, C., Chusri, P., Fusco, D.N., et al. (2014). Kinetic differences in the induction of interferon stimulated genes by interferon-α and interleukin 28B are altered by infection with hepatitis C virus. Hepatology *59*, 1250–1261.

Kane, M., Yadav, S.S., Bitzegeio, J., Kutluay, S.B., Zang, T., Wilson, S.J., Schoggins, J.W., Rice, C.M., Yamashita, M., Hatziioannou, T., and Bieniasz, P.D. (2013). MX2 is an interferon-induced inhibitor of HIV-1 infection. Nature *502*, 563–566.

Kane, M., Zang, T.M., Rihn, S.J., Zhang, F., Kueck, T., Alim, M., Schoggins, J., Rice, C.M., Wilson, S.J., and Bieniasz, P.D. (2016). Identification of interferon-stimulated genes with antiretroviral activity. Cell Host Microbe *20*, 392–405.

Keele, B.F., Van Heuverswyn, F., Li, Y., Bailes, E., Takehisa, J., Santiago, M.L., Bibollet-Ruche, F., Chen, Y., Wain, L.V., Liegeois, F., et al. (2006). Chimpanzee reservoirs of pandemic and nonpandemic HIV-1. Science *313*, 523–526.

Kirchhoff, F. (2010). Immune evasion and counteraction of restriction factors by HIV-1 and other primate lentiviruses. Cell Host Microbe *8*, 55–67.

Klein, J.S., and Bjorkman, P.J. (2010). Few and far between: how HIV may be evading antibody avidity. PLoS Pathog. *6*, e1000908.

Kluge, S.F., Sauter, D., Vogl, M., Peeters, M., Li, Y., Bibollet-Ruche, F., Hahn, B.H., and Kirchhoff, F. (2013). The transmembrane domain of HIV-1 Vpu is sufficient to confer anti-tetherin activity to SIVcpz and SIVgor Vpu proteins: cytoplasmic determinants of Vpu function. Retrovirology *10*, 32.

Kluge, S.F., Sauter, D., and Kirchhoff, F. (2015). SnapShot: antiviral restriction factors. Cell *163*, 774–774.e1.

Kmiec, D., Iyer, S.S., Stürzel, C.M., Sauter, D., Hahn, B.H., and Kirchhoff, F. (2016). Vpu-mediated counteraction of tetherin is a major determinant of HIV-1 interferon resistance. MBio *7*, e00934-16.

Krapp, C., Hotter, D., Gawanbacht, A., McLaren, P.J., Kluge, S.F., Stürzel, C.M., Mack, K., Reith, E., Engelhart, S., Ciuffi, A., et al. (2016). Guanylate binding protein (GBP) 5 is an interferon-inducible inhibitor of HIV-1 infectivity. Cell Host Microbe *19*, 504–514.

Langmead, B., and Salzberg, S.L. (2012). Fast gapped-read alignment with Bowtie 2. Nat. Methods *9*, 357–359.

Levin, D., Schneider, W.M., Hoffmann, H.H., Yarden, G., Busetto, A.G., Manor, O., Sharma, N., Rice, C.M., and Schreiber, G. (2014). Multifaceted activities of type I interferon are revealed by a receptor antagonist. Sci. Signal. *7*, ra50.

Li, Y., Kappes, J.C., Conway, J.A., Price, R.W., Shaw, G.M., and Hahn, B.H. (1991). Molecular characterization of human immunodeficiency virus type 1 cloned directly from uncultured human brain tissue: identification of replication-competent and -defective viral genomes. J. Virol. *65*, 3973–3985.

Liao, Y., Smyth, G.K., and Shi, W. (2013). The Subread aligner: fast, accurate and scalable read mapping by seed-and-vote. Nucleic Acids Res. *41*, e108.

Liberatore, R.A., and Bieniasz, P.D. (2011). Tetherin is a key effector of the antiretroviral activity of type I interferon *in vitro* and *in vivo*. Proc. Natl. Acad. Sci. USA *108*, 18097–18101.

Love, M.I., Huber, W., and Anders, S. (2014). Moderated estimation of fold change and dispersion for RNA-seq data with DESeq2. Genome Biol. *15*, 550.

Mali, P., Yang, L., Esvelt, K.M., Aach, J., Guell, M., DiCarlo, J.E., Norville, J.E., and Church, G.M. (2013). RNA-guided human genome engineering via Cas9. Science *339*, 823–826.

Matheson, N.J., Sumner, J., Wals, K., Rapiteanu, R., Weekes, M.P., Vigan, R., Weinelt, J., Schindler, M., Antrobus, R., Costa, A.S., et al. (2015). Cell surface proteomic map of HIV infection reveals antagonism of amino acid metabolism by Vpu and Nef. Cell Host Microbe *18*, 409–423.

Miyoshi, H., Blömer, U., Takahashi, M., Gage, F.H., and Verma, I.M. (1998). Development of a self-inactivating lentivirus vector. J. Virol. *72*, 8150–8157.

Nakano, Y., Misawa, N., Juarez-Fernandez, G., Moriwaki, M., Nakaoka, S., Funo, T., Yamada, E., Soper, A., Yoshikawa, R., Ebrahimi, D., et al. (2017). HIV-1 competition experiments in humanized mice show that APOBEC3H imposes selective pressure and promotes virus adaptation. PLoS Pathog. *13*, e1006348.

Neil, S.J., Sandrin, V., Sundquist, W.I., and Bieniasz, P.D. (2007). An interferon-α-induced tethering mechanism inhibits HIV-1 and Ebola virus particle release but is counteracted by the HIV-1 Vpu protein. Cell Host Microbe *2*, 193–203.

Neil, S.J., Zang, T., and Bieniasz, P.D. (2008). Tetherin inhibits retrovirus release and is antagonized by HIV-1 Vpu. Nature *451*, 425–430.

Nie, C., Sato, K., Misawa, N., Kitayama, H., Fujino, H., Hiramatsu, H., Heike, T., Nakahata, T., Tanaka, Y., Ito, M., and Koyanagi, Y. (2009). Selective infection of CD4+ effector memory T lymphocytes leads to preferential depletion of memory T lymphocytes in R5 HIV-1-infected humanized NOD/SCID/IL-2Rγ^{null} mice. Virology *394*, 64–72.

Nowak, M., and May, R.M. (2000). Virus Dynamics: Mathematical Principles of Immunology and Virology: Mathematical Principles of Immunology and Virology (Oxford University Press).

Ohtomo, T., Sugamata, Y., Ozaki, Y., Ono, K., Yoshimura, Y., Kawai, S., Koishihara, Y., Ozaki, S., Kosaka, M., Hirano, T., and Tsuchiya, M. (1999). Molecular cloning and characterization of a surface antigen preferentially overexpressed on multiple myeloma cells. Biochem. Biophys. Res. Commun. *258*, 583–591.

Parrish, N.F., Gao, F., Li, H., Giorgi, E.E., Barbian, H.J., Parrish, E.H., Zajic, L., Iyer, S.S., Decker, J.M., Kumar, A., et al. (2013). Phenotypic properties of transmitted founder HIV-1. Proc. Natl. Acad. Sci. USA *110*, 6626–6633.

Sandler, N.G., Bosinger, S.E., Estes, J.D., Zhu, R.T., Tharp, G.K., Boritz, E., Levin, D., Wijeyesinghe, S., Makamdop, K.N., del Prete, G.Q., et al. (2014). Type I interferon responses in rhesus macaques prevent SIV infection and slow disease progression. Nature *511*, 601–605.

Sato, K., Yamamoto, S.P., Misawa, N., Yoshida, T., Miyazawa, T., and Koyanagi, Y. (2009). Comparative study on the effect of human BST-2/Tetherin on HIV-1 release in cells of various species. Retrovirology *6*, 53.

Sato, K., Izumi, T., Misawa, N., Kobayashi, T., Yamashita, Y., Ohmichi, M., Ito, M., Takaori-Kondo, A., and Koyanagi, Y. (2010). Remarkable lethal G-to-A mutations in vif-proficient HIV-1 provirus by individual APOBEC3 proteins in humanized mice. J. Virol. *84*, 9546–9556.

Sato, K., Misawa, N., Fukuhara, M., Iwami, S., An, D.S., Ito, M., and Koyanagi, Y. (2012). Vpu augments the initial burst phase of HIV-1 propagation and downregulates BST2 and CD4 in humanized mice. J. Virol. *86*, 5000–5013.

Sato, K., Misawa, N., Iwami, S., Satou, Y., Matsuoka, M., Ishizaka, Y., Ito, M., Aihara, K., An, D.S., and Koyanagi, Y. (2013). HIV-1 Vpr accelerates viral replication during acute infection by exploitation of proliferating CD4+ T cells in vivo. PLoS Pathog. *9*, e1003812.

Sato, K., Takeuchi, J.S., Misawa, N., Izumi, T., Kobayashi, T., Kimura, Y., Iwami, S., Takaori-Kondo, A., Hu, W.S., Aihara, K., et al. (2014). APOBEC3D and APOBEC3F potently promote HIV-1 diversification and evolution in humanized mouse model. PLoS Pathog. *10*, e1004453.

Sauter, D., Schindler, M., Specht, A., Landford, W.N., Münch, J., Kim, K.A., Votteler, J., Schubert, U., Bibollet-Ruche, F., Keele, B.F., et al. (2009). Tetherin-driven adaptation of Vpu and Nef function and the evolution of pandemic and nonpandemic HIV-1 strains. Cell Host Microbe *6*, 409–421.

Sauter, D., Unterweger, D., Vogl, M., Usmani, S.M., Heigele, A., Kluge, S.F., Hermkes, E., Moll, M., Barker, E., Peeters, M., et al. (2012). Human tetherin exerts strong selection pressure on the HIV-1 group N Vpu protein. PLoS Pathog. *8*, e1003093.

Sauter, D., Hotter, D., Van Driessche, B., Stürzel, C.M., Kluge, S.F., Wildum, S., Yu, H., Baumann, B., Wirth, T., Plantier, J.C., et al. (2015). Differential regulation of NF-κB-mediated proviral and antiviral host gene expression by primate lentiviral Nef and Vpu proteins. Cell Rep. *10*, 586–599.

Schubert, U., Clouse, K.A., and Strebel, K. (1995). Augmentation of virus secretion by the human immunodeficiency virus type 1 Vpu protein is cell type independent and occurs in cultured human primary macrophages and lymphocytes. J. Virol. *69*, 7699–7711.

Schubert, U., Bour, S., Willey, R.L., and Strebel, K. (1999). Regulation of virus release by the macrophage-tropic human immunodeficiency virus type 1 AD8 isolate is redundant and can be controlled by either Vpu or Env. J. Virol. *73*, 887–896.

Shah, A.H., Sowrirajan, B., Davis, Z.B., Ward, J.P., Campbell, E.M., Planelles, V., and Barker, E. (2010). Degranulation of natural killer cells following interaction with HIV-1-infected cells is hindered by downmodulation of NTB-A by Vpu. Cell Host Microbe *8*, 397–409.

Shirazi, Y., and Pitha, P.M. (1992). Alpha interferon inhibits early stages of the human immunodeficiency virus type 1 replication cycle. J. Virol. *66*, 1321–1328.

Shultz, L.D., Brehm, M.A., Garcia-Martinez, J.V., and Greiner, D.L. (2012). Humanized mice for immune system investigation: progress, promise and challenges. Nat. Rev. Immunol. *12*, 786–798.

Simon, V., Bloch, N., and Landau, N.R. (2015). Intrinsic host restrictions to HIV-1 and mechanisms of viral escape. Nat. Immunol. *16*, 546–553.

Soper, A., Juarez-Fernandez, G., Aso, H., Moriwaki, M., Yamada, E., Nakano, Y., Koyanagi, Y., and Sato, K. (2017). Various plus unique: viral protein U as a plurifunctional protein for HIV-1 replication. Exp. Biol. Med. (Maywood) *242*, 850–858.

Sugden, S., and Cohen, E.A. (2015). Attacking the supply lines: HIV-1 restricts alanine uptake to prevent T cell activation. Cell Host Microbe *18*, 514–517.

Sun, J., Nishiyama, T., Shimizu, K., and Kadota, K. (2013). TCC: an R package for comparing tag count data with robust normalization strategies. BMC Bioinformatics *14*, 219.

Theodore, T.S., Englund, G., Buckler-White, A., Buckler, C.E., Martin, M.A., and Peden, K.W. (1996). Construction and characterization of a stable full-length macrophage-tropic HIV type 1 molecular clone that directs the production of high titers of progeny virions. AIDS Res. Hum. Retroviruses *12*, 191–194.

Trapnell, C., Pachter, L., and Salzberg, S.L. (2009). TopHat: discovering splice junctions with RNA-Seq. Bioinformatics *25*, 1105–1111.

Van Damme, N., Goff, D., Katsura, C., Jorgenson, R.L., Mitchell, R., Johnson, M.C., Stephens, E.B., and Guatelli, J. (2008). The interferon-induced protein BST-2 restricts HIV-1 release and is downregulated from the cell surface by the viral Vpu protein. Cell Host Microbe *3*, 245–252.

Vigan, R., and Neil, S.J. (2010). Determinants of tetherin antagonism in the transmembrane domain of the human immunodeficiency virus type 1 Vpu protein. J. Virol. *84*, 12958–12970.

Wei, X., Decker, J.M., Liu, H., Zhang, Z., Arani, R.B., Kilby, J.M., Saag, M.S., Wu, X., Shaw, G.M., and Kappes, J.C. (2002). Emergence of resistant human immunodeficiency virus type 1 in patients receiving fusion inhibitor (T-20) monotherapy. Antimicrob. Agents Chemother. *46*, 1896–1905.

Willey, R.L., Maldarelli, F., Martin, M.A., and Strebel, K. (1992). Human immunodeficiency virus type 1 Vpu protein induces rapid degradation of CD4. J. Virol. *66*, 7193–7200.

Yamada, E., Yoshikawa, R., Nakano, Y., Misawa, N., Koyanagi, Y., and Sato, K. (2015). Impacts of humanized mouse models on the investigation of HIV-1 infection: illuminating the roles of viral accessory proteins in vivo. Viruses *7*, 1373–1390.

Yu, G., and He, Q.Y. (2016). ReactomePA: an R/Bioconductor package for reactome pathway analysis and visualization. Mol. Biosyst. *12*, 477–479.

Yu, G., Wang, L.G., Han, Y., and He, Q.Y. (2012). clusterProfiler: an R package for comparing biological themes among gene clusters. OMICS *16*, 284–287.

STAR★METHODS

KEY RESOURCES TABLE

REAGENT or RESOURCE	SOURCE	IDENTIFIER
Antibodies		
FITC-conjugated anti-CD3	Biolegend	Cat# 300406; RRID :AB_314060
PE-conjugated anti-CD3	BD Biosciences	Cat# 555333; RRID: AB_395740
APC-conjugated anti-CD4	Biolegend	Cat# 300514; RRID: AB_314082
APC-conjugated anti-CD4	Thermo Fisher Scientific	Cat# MHCD0405; RRID: AB_10373698
APC-conjugated anti-CD8	Dako	Cat# C722701; RRID: AB_578594
APC/Cy7-conjugated anti-CD8	Biolegend	Cat# 344714; RRID: AB_2044006
PE-conjugated anti-CD45	Biolegend	Cat# 304008; RRID: AB_314396
PerCP/Cy5.5-conjugated anti-CD45	Biolegend	Cat# 368504; RRID: AB_2566352
PerCP/Cy5.5-conjugated anti-CD45RA	Biolegend	Cat# 304121; RRID: AB_893358
APC-conjugated anti-ISG15	R&D Systems	Cat# IC8044A
APC-conjugated anti-Tetherin	Biolegend	Cat# 348410; RRID: AB_2067121
FITC-conjugated anti-CCR5	BD Biosciences	Cat# 555992; RRID: AB_396278
APC-conjugated anti-SLAMF6	R&D Systems	Cat# FAB19081A; RRID: AB_884369
PE-conjugated anti-PVR	Biolegend	Cat# 337610; RRID: AB_2174019
Anti-HLA-C	Millipore	Cat# MABF233; RRID: AB_2687888
Anti-SLC38A1	Santa Cruz Biotechnology	Cat# sc-67080; RRID: AB_2190399
Alexa Fluor 647-conjugated anti-IκB	BD Biosciences	Cat# 560817; RRID: AB_2033974
Alexa Fluor 647-conjugated anti-mouse IgG	Thermo Fisher Scientific	Cat# A-21237; RRID: AB_2535806
Alexa Fluor 647-conjugated anti-rabbit IgG	Thermo Fisher Scientific	Cat# A-21245; RRID: AB_2535813
FITC-conjugated anti-HIV-1 p24 (clone KC57)	Beckman Coulter	Cat# 6604665
Anti-HIV-1 Env (clone 16H3)	NIH AIDS Reagent Program	Cat# 12559
Anti-HIV-1 p24	Abcam	Cat# ab9071; RRID: AB_306981
Anti-Tetherin	(Ohtomo et al., 1999)	N/A
Anti-alpha-Tubulin	Sigma-Aldrich	Cat# T9026; RRID: AB_477593
Bacterial and Virus Strains		
HIV-1 strain AD8	(Theodore et al., 1996)	Genbank accession no. AF004394.1
HIV-1 strain REJO	(Parrish et al., 2013)	N/A
HIV-1 strain STCO1	(Parrish et al., 2013)	N/A
SIVcpz strain EK505	(Bibollet-Ruche et al., 2012; Keele et al., 2006)	Genbank accession no. JN835460.1
Biological Samples		
Human CD34$^+$ hematopoietic stem cells	UCLA CFAR Gene and Cellular Therapy Core Facility	http://aidsinstitute.ucla.edu/cfar/gene-and-cellular-therapy-core
Human PBMCs	This study	
Human peripheral CD4$^+$ T cells	This study	
Chemicals, Peptides, and Recombinant Proteins		
L-glutamate	Thermo Fisher Scientific	Cat# 25030081
Ficoll-Paque	GE Healthcare	Cat# 17-1440-03
RosetteSep Human CD4$^+$ T Cell enrichment cocktail	STEMCELL technologies	Cat# 15022
Phytohemagglutinin	Sigma-Aldrich	Cat# 11082132001
Human interleukin-2 IS	Miltenyi Biotec	Cat# 130-097-745
Protein loading dye	LI-COR	Cat# 928-40004
Human IFN-α	Sigma-Aldrich	Cat# I4784
Pegylated human IFN-α2a (Pegasys®)	Chugai Pharmaceutical co.	N/A

(*Continued on next page*)

Continued

REAGENT or RESOURCE	SOURCE	IDENTIFIER
IFN-1ant	(Levin et al., 2014)	N/A
Coelenterazine (native-CTZ)	PJK	Cat# 102173
SuperScript III reverse transcriptase	Thermo Fisher Scientific	Cat# 18080085
DNase I	Thermo Fisher Scientific	Cat# 18047019
RNaseOUT	Thermo Fisher Scientific	Cat# 10777019
PrimeSTAR GXL DNA polymerase	Takara	Cat# R050A
*Afl*II	Takara	Cat# 1236A
Critical Commercial Assays		
HIV-1 p24 antigen ELISA kit	ZetroMetrix	Cat# 0801111
Gal-Screen β-galactosidase reporter assay system	Thermo Fisher Scientific	Cat# T1028
Luciferase assay system	Promega	Cat# E1501
QIAamp RNA blood mini kit	Qiagen	Cat# 52304
QIAamp viral RNA mini kit	Qiagen	Cat# 52906
Zero blunt TOPO PCR cloning kit	Thermo Fisher Scientific	Cat# K280002
Deposited Data		
Transcriptome data (RNA-seq)	This study	GEO: GSE94776
Experimental Models: Cell Lines		
Human: HEK293T cells	ATCC	CRL-1573
Human: TZM-bl cells	NIH AIDS Reagent Program	Cat# 8129
Human: Jurkat cells	Lab strain	N/A
Human: Jurkat *BST2*_g2-10 cells	This study	N/A
Experimental Models: Organisms/Strains		
Mouse: NOD.Cg-*Prkdc*^{scid} *Il2rg*^{tm1Sug}/Jic (NOG)	Central Institute for Experimental Animals	https://www.ciea.or.jp/en/nog_mouse.html
Oligonucleotides		
Primers for IMC construction, see Table S6	This study	N/A
Primers for RT-PCR and quantitative RT-PCR, see Table S6	This study	N/A
CRISPR gRNA targeting *BST2*-F: 5'-ttt ctt ggc ttt ata tat ctt gtg gaa agg acg aaa cac cGG ACG GCC TTC GGG CAG TGA-3'	This study	N/A
CRISPR gRNA targeting *BST2*-R: 5'-gac tag cct tat ttt aac ttg cta ttt cta gct caa aac TCA CTG CCC GAA GGC CGT CC-3'	This study	N/A
Recombinant DNA		
Plasmid: pAD8^{+} (IMC of HIV-1 AD8 WT)	(Theodore et al., 1996)	Genbank accession no. AF004394.1
Plasmid: pAD8-U_{DEL2} (IMC of HIV-1 AD8Δ*vpu*)	(Schubert et al., 1999; Schubert et al., 1995)	N/A
Plasmid: pREJO.c_TOPO-XL #2624 (IMC of HIV-1 REJO WT)	NIH AIDS Reagent Program (Parrish et al., 2013)	Cat# 11746
Plasmid: pREJO.c_TOPO-XL #2624 A15L (IMC of HIV-1 REJO A15L)	This study	N/A
Plasmid: pREJO.c_TOPO-XL #2624 *vpu* stop (IMC of HIV-1 REJO *vpu* stop)	This study	N/A
Plasmid: pSTCOr1 (IMC of HIV-1 STCO1 WT)	NIH AIDS Reagent Program (Parrish et al., 2013)	Cat# 12417
Plasmid: pSTCOr1 A15L/A19L (IMC of HIV-1 STCO1 A15L/A19L)	This study	N/A
Plasmid: pSTCOr1 R45K (IMC of HIV-1 STCO1 R45K)	This study	N/A

(*Continued on next page*)

Continued

REAGENT or RESOURCE	SOURCE	IDENTIFIER
Plasmid: pSTCOr1 *vpu* stop (IMC of HIV-1 STCO1 *vpu* stop)	This study	N/A
Plasmid: pEK505 (IMC of SIVcpz EK505 WT)	(Keele et al., 2006)	Genbank accession no. JN835460.1
Plasmid: pEK505 AVSIA/LL (IMC of SIVcpz EK505 AVSIA/LL)	This study	N/A
Plasmid: pEK505 *vpu* stop (IMC of SIVcpz EK505 *vpu* stop)	This study	N/A
Plasmid: pCG-Vpu	(Sauter et al., 2009)	N/A
Plasmid: pCG-GBP5	(Krapp et al., 2016)	N/A
Plasmid: pCG-tetherin	(Sauter et al., 2009)	N/A
Plasmid: pHIT-G_VSVg	(Fouchier et al., 1997)	xxx
Plasmid: constitutively active mutant of IKKβ	Bernd Baumann (Hotter et al., 2013)	N/A
Plasmid: pNF-κB(3x)-firefly luciferase	Bernd Baumann (Hotter et al., 2013)	N/A
Plasmid: pTAL-*Gaussia* luciferase	(Hotter et al., 2013)	N/A
Plasmid: gRNA_cloning plasmid	Addgene	Cat# 41824
Plasmid: phCas9	Addgene	Cat# 41815
Plasmid: CCR5 expression lentiviral plasmid	This study	N/A
Plasmid: pCAG-HIVgp	Miyoshi et al., 1998	N/A
Plasmid: pCMV-VSV-G-RSV-Rev	Miyoshi et al., 1998	N/A
Plasmid: pCRII-blunt-TOPO	Thermo Fisher Scientific	N/A
Software and Algorithms		
CellQuest	BD Biosciences	N/A
FACSDiva	BD Biosciences	http://www.bdbiosciences.com/jp/instruments/software/facsdiva/
FlowJo	Tree Star	https://www.flowjo.com
Bowtie2	Langmead and Salzberg, 2012	http://bowtie-bio.sourceforge.net/bowtie2/index.shtml
Tophat2	Trapnell et al., 2009	http://ccb.jhu.edu/software/tophat/index.shtml
R Statistical Computing software	The R Foundation	https://www.r-project.org
Rsubread	Liao et al., 2013	http://bioconductor.org/packages/release/bioc/html/Rsubread.html
TCC	Sun et al., 2013	http://bioconductor.org/packages/release/bioc/html/TCC.html
DESeq2	Love et al., 2014	https://bioconductor.org/packages/release/bioc/html/DESeq2.html
clusterProfiler	Yu et al., 2012	https://bioconductor.org/packages/release/bioc/html/clusterProfiler.html
ReactomePA	Yu and He, 2016	http://bioconductor.org/packages/release/bioc/html/ReactomePA.html
gplots	Gregory R. Warnes	https://cran.r-project.org/web/packages/gplots/index.html
GraphPad Prism	GraphPad Software	https://www.graphpad.com/scientific-software/prism/
Other		
Pestle homogenizer	Bio-bik	Cat# 1004-39
0.45-μm-pore-size filter	Merck Millipore	Cat# SLHV033RB

CONTACT FOR REAGENT AND RESOURCE SHARING

Further information and requests for resources and reagents may be directed to and will be fulfilled by the Lead Contact, Kei Sato (ksato@virus.kyoto-u.ac.jp).

EXPERIMENTAL MODEL AND SUBJECT DETAILS

Ethics Statement

All animal studies were conducted following the guidelines for the Care and Use of Laboratory Animals of the Ministry of Education, Culture, Sports, Science and Technology, Japan. The authors received approval from the Institutional Animal Care and Use Committees (IACUC)/ethics committee of the institutional review board of Kyoto University (protocol number A16-3-2). All protocols involving human subjects were reviewed and approved by the Kyoto University institutional review board. All human subjects provided written informed consent.

Humanized Mice

NOD.Cg-*Prkdc*^{scid} *Il2rg*^{tm1Sug}/Jic (NOG) mice (Ito et al., 2002) were obtained from the Central Institute for Experimental Animals (Kanagawa, Japan). The mice were maintained under specific-pathogen-free conditions and were handled in accordance with the Regulation on Animal Experimentation at Kyoto University. Human CD34$^+$ hematopoietic stem cells were isolated from human fetal liver and provided from Dr. Dong Sung An (University of California, Los Angeles, USA). Humanized mice (NOG-hCD34 mice) were generated as previously described (Nakano et al., 2017; Nie et al., 2009; Sato et al., 2010; Sato et al., 2012; Sato et al., 2013; Sato et al., 2014). Briefly, 83 new-born (aged 0 to 2 days) NOG mice from 33 litters were irradiated (10 cGy per mouse) by an RX-650 X-ray cabinet system (Faxitron X-ray Corporation) and were then intrahepatically injected with the obtained human CD34$^+$ cells (8×10^4 to 30×10^4 cells; 19 donors).

Cells and Viruses

HEK293T cells (a human embryonic kidney cell line; ATCC CRL-1573) and TZM-bl cells (obtained through the NIH AIDS Research and Reference Reagent Program) (Wei et al., 2002) were maintained in Dulbecco's modified Eagle's medium (Sigma) containing FCS, 2 mM L-glutamate (Thermo Fisher Scientific) and antibiotics. HEK293T cells were transfected using a standard calcium phosphate protocol. Human peripheral mononuclear cells (PBMCs) were isolated from human PB using Ficoll-Paque (GE Healthcare) according to the manufacturer's protocol. CD4$^+$ T cells were isolated using the RosetteSep Human CD4$^+$ T Cell Enrichment Cocktail (STEMCELL technologies) according to manufacturer's instructions. Jurkat cells (a human CD4$^+$ T cell line) and primary cells activated with phytohemagglutinin (PHA) (Sigma) were maintained in RPMI1640 (Sigma) containing FCS and antibiotics with human interleukin-2 (100 U/ml) (Miltenyi Biotec) as previously described (Sato et al., 2012).

The infectious molecular clones (IMCs) of HIV-1 strain AD8 (pAD8$^+$) (Theodore et al., 1996) and *vpu*-deleted AD8 (pAD8-U$_{DEL2}$, which carries an 81 bp-deletion and an irrelevant 8-bp insertion in the *vpu* region) (Schubert et al., 1999; Schubert et al., 1995) were kindly provided by Dr. Klaus Strebel (National Institute of Health, USA). The IMCs of HIV-1 strains REJO (a transmitted founder virus) (Parrish et al., 2013) and STCO1 (a chronic control virus) (Parrish et al., 2013), and SIVcpz strain EK505 (Keele et al., 2006) were kindly provided by Dr. Beatrice H Hahn (University of Pennsylvania, USA). The derivatives of these viruses were generated by mutagenesis/overlap extension PCR using the primers listed in Table S6. For virus preparation, HEK293T cells were transfected with proviral DNA using the calcium phosphate method. In some experiments, an expression plasmid encoding the vesicular stomatitis virus glycoprotein (VSV-G) was co-transfected in a DNA ratio of 1:5 (VSV-G:proviral DNA) for pseudotyping. At 48 h post-transfection, the culture supernatants were harvested, centrifuged, and then filtered through a 0.45-μm-pore-size filter. To titrate virus infectivity, the prepared virus was serially diluted and then inoculated onto PHA-stimulated human PBMCs in a 96-well plate in triplicates. At 14 days post-infection, the endpoint was determined using an HIV-1 p24 antigen enzyme-linked immunosorbent assay (ELISA) kit (ZetroMetrix), and virus infectivity was calculated as the 50% tissue culture infectious doses (TCID$_{50}$) according to the Reed-Muench method.

METHOD DETAILS

Expression Plasmids

Vpu, GBP5 and tetherin were expressed from CMV promoter-driven pCG vectors coexpressing eGFP or DsRed2 via an IRES. The expression plasmid for a constitutively active mutant of IKKβ and the NF-κB firefly luciferase reporter were kindly provided by Dr. Bernd Baumann (Ulm University, Germany) (Sauter et al., 2015). The pTAL-*Gaussia* luciferase control vector was generated by replacing the firefly luciferase gene in a reporter vector purchased from Clontech (catalog #63190).

Western Blotting

To quantify relative Env levels by Western blotting, HEK293T cells were transfected with proviral DNA using the calcium phosphate method. Two days later, cell-free virions were purified by centrifugation of cell culture supernatants through a 20% sucrose cushion at 20,800 g for 90 minutes at 4°C and lysed in a mixture of 75% Western blot lysis buffer (150 mM NaCl, 50 mM HEPES, 5 mM EDTA,

0.1% (v/v) NP-40, 500 μM Na_3VO_4, 500 μM NaF, pH 7.5), 22.5% Protein Loading Dye (LI-COR) and 2.5% β-mercaptoethanol. After heating at 95°C for 5 minutes, lysates were separated on NuPAGE 4-12% Bis-Tris Gels (Invitrogen) and blotted onto Immobilon-FL PVDF membranes (Merck Millipore). Proteins were stained using primary antibodies directed against HIV-1 Env (obtained through the NIH AIDS Reagent Program, Division of AIDS, NIAID, NIH: 16H3 mAb from Drs. Barton F. Haynes and Hua-Xin Liao), p24 (Abcam #ab9071) and Infrared Dye labeled secondary antibodies (LI-COR IRDye). Proteins were detected using the infrared imager Odyssey9120 (LI-COR) or ChemiDoc Touch Imaging System (Bio-Rad), and band intensities were quantified using Image Studio Lite Version 4.0 (LI-COR). To detect cellular proteins (tetherin and Tubulin), proteins were stained using primary antibodies directed against tetherin (Chugai Pharmaceutical Co., Japan) (Ohtomo et al., 1999; Sato et al., 2009; Van Damme et al., 2008) and Tubulin (DM1A; Sigma).

TZM-bl Reporter Assay and Virion Infectivity

Infectious HIV-1 yield was determined using TZM-bl indicator cells. Briefly, 6,000 cells were seeded in 96-well plates and infected in triplicates with cell culture supernatants. Three days later, infection rates were measured using a Gal-Screen β-galactosidase reporter assay system (Thermo Fisher Scientific) according to the manufacturer's instructions. β-galactosidase activities were quantified as relative light units per second (RLU/s) using an Orion Microplate Luminometer. To determine virion infectivity, infectious virus yield was normalized to the p24 content in the same samples. p24 concentrations were determined using a home-made HIV-1 p24 ELISA.

NF-κB Reporter Assay

To determine NF-κB activity in the presence of HIV-1 or SIVcpz, HEK293T cells were cotransfected with a firefly luciferase reporter construct under the control of three NF-κB binding sites (100 ng), a *Gaussia* luciferase construct under the control of a constitutively active pTAL promoter (5 ng) for normalization, and an IMC of HIV-1 or SIVcpz. To activate NF-κB, a constitutively active mutant of IKKβ (40 ng) was cotransfected. Cells were seeded in 96-well plates coated with poly-L-lysine and transfected in triplicates using a standard calcium phosphate transfection protocol. 40 h post-transfection, a dual luciferase assay (Promega and PJK GmbH) was performed and the firefly luciferase signals were normalized to the corresponding *Gaussia* luciferase control values.

Generation of Tetherin KO Jurkat Cells by Using CRISPR-Cas9 System

The CCR5-expressing tetherin KO Jurkat cell line was prepared using the CRISPR-Cas9 system (Ebina et al., 2013; Mali et al., 2013). Briefly, the following oligonucleotides were prepared to produce the guide RNA (gRNA) targeting *BST2* gene (encoding tetherin): gRNA-BST2-F, 5'-ttt ctt ggc ttt ata tat ctt gtg gaa agg acg aaa cac cGG ACG GCC TTC GGG CAG TGA-3'; gRNA-BST2-R, 5'-gac tag cct tat ttt aac ttg cta ttt cta gct caa aac TCA CTG CCC GAA GGC CGT CC-3'. These oligonucleotides were annealed and inserted into the *Afl*II site of the gRNA_cloning plasmid (Addgene #41824; a U6 target gRNA expression plasmid). Subsequently, Jurkat cells were co-transfected with this plasmid and an hCas9-expressing plasmid (Addgene #41815) in a DNA ratio of 1:1 using the Neon Transfection system (Thermo Fisher Scientific). The transfected Jurkat cells were treated with human IFN-α (1,000 unit/ml; Sigma) for 48 h, Then, the cells were stained with an anti-tetherin-APC antibody (Biolegend) and tetherin-negative cells were sorted by FACSAria (BD Biosciences). Clonal cell lines were established by serial dilution and lack of tetherin expression was validated by flow cytometry and Western blotting. Furthermore, partial deletion of the *BST2* gene was confirmed by sequencing, and the Jurkat clone, *BST2*_g2-10, was used for further study. To stably express CCR5, a CCR5-expressing lentiviral vector was prepared as previously described (Ebina et al., 2013). Briefly, HEK293T cells were co-transfected with a CCR5-expressing genomic plasmid and helper plasmids, pCAG-HIVgp and pCMV-VSV-G-RSV-Rev (kindly provided by Dr. Hiroyuki Miyoshi [Keio University, Japan]) using a standard calcium phosphate transfection protocol (Miyoshi et al., 1998). At 48 h post-transfection, the culture supernatant was harvested, centrifuged, and filtered through a 0.45-μm-pore-size filter. Then, the Jurkat *BST2*_g2-10 cells were transduced with this CCR5-expressing lentiviral vector. At 48 h post-transduction, the cells were stained with an anti-CCR5-FITC antibody (BD Biosciences) and the CCR5-expressing population was sorted by FACSJazz (BD Biosciences). To investigate the viral replication kinetics in Jurkat *BST2*_g2-10 cells, viruses were inoculated at multiplicity of infection (MOI) 0.1 and the amount of viral p24 antigen in the culture supernatant was routinely monitored by p24 ELISA.

Infection of Humanized Mice and *In Vivo* Competition Assay

WT AD8 and AD8Δ*vpu* (1,500 $TCID_{50}$) were intraperitoneally inoculated into humanized mice (Figure 1). PB was collected at 0, 1, 2, 3, 5, 7, 9, 12 and 15 wpi from the retro-orbital venous plexus under anesthesia. At 15 wpi, these mice were euthanized and sacrificed, and the human mononuclear cells (MNCs) in PB, spleen, bone marrow, mesenteric lymph nodes and their fluids were collected as previously described (Nakano et al., 2017; Nie et al., 2009; Sato et al., 2010; Sato et al., 2012; Sato et al., 2013; Sato et al., 2014). For the *in vivo* competition assays (Figures 3, 4, and 6) (Nakano et al., 2017), each virus preparation (equivalent to 1,000 $TCID_{50}$) was intraperitoneally inoculated into humanized mice. RPMI1640 was used for mock infection. At 2 wpi, these mice were euthanized and sacrificed, and the human MNCs in PB, spleen, bone marrow, mesenteric lymph nodes and their fluids were collected as previously described (Nakano et al., 2017; Nie et al., 2009; Sato et al., 2010; Sato et al., 2012; Sato et al., 2013; Sato et al., 2014). Briefly, PB was taken via cardiac puncture, and spleens were crushed and rubbed on a steal mesh with 1-mm grids to generate single cell suspensions in RPMI 1640 supplemented with 4% FCS. Lymph nodes were gently homogenized in RPMI 1640 supplemented with 4% FCS using a pestle homogenizer (Bio-bik). To collect bone marrow, thighbones were dissected at both ends and the interior was

flushed with RPMI 1640 supplemented with 4% FCS. To collect the fluid of the respective organs, cell suspensions obtained from respective organs were centrifuged, and the supernatants were filtered through a 0.45-μm-pore-size filter (Merck Millipore).

Infection of Primary Cells *Ex Vivo*

To investigate modulation of cellular protein levels by the virus, PBMCs and $CD4^+$ T cells were infected via spinoculation. Briefly, 1.5×10^6 cells were seeded in 100 μl supplemented medium in a 96-well plate and 150 μl virus stock was added to each well. After centrifugation at 1,200 g for 2 h at 37°C, the cells were resuspended and transferred to 6-well plates. 72 h post infection, the cells were harvested and stained for flow cytometry. For quantification of HIV-1/SIVcpz p24, IκB and SLC38A1, cells were permeabilized before staining.

RNA Extraction, RT-PCR, TOPO Cloning and Sanger Sequencing

RNA was extracted from human MNCs using QIAamp RNA blood mini kit (Qiagen) and from plasma and fluids using QIAamp viral RNA mini kit (Qiagen) according to the manufacturer's protocol. cDNA was prepared by using SuperScript III reverse transcriptase (Thermo Fisher Scientific) with DNase I (Thermo Fisher Scientific) and RNaseOUT (Thermo Fisher Scientific). To amplify the *vpu*-encoding region, RT-PCR was performed by using the primers listed in Table S6 and PrimeSTAR GXL DNA polymerase (Takara) according to the manufacture's protocol. RT-PCR products were cloned into pCRII-blunt-TOPO by using Zero blunt TOPO PCR cloning kit (Thermo Fisher Scientific) according to the manufacture's protocol. The sequence data were analyzed by Sequencher v5.1 software (Gene Codes Corporation).

Quantitative RT-PCR

The amount of HIV-1 RNA in 50 μl plasma was quantified by Bio Medical Laboratories, Inc. (the detection limit of HIV-1 RNA is 800 copies/ml). The amounts of HIV-1 RNA in tissues and fluids were quantified by real-time RT-PCR using the primers listed in Table S6 and the CFX Connect Real-Time System (Bio-Rad). The mRNA expression levels of cellular genes (*BST2*, *IFI44L*, *ISG15*, *APOBEC3G*, *MX1*, *IFI6* and *GAPDH*) were measured by real-time RT-PCR using the primers listed in Table S6 and the CFX Connect Real-Time System (Bio-Rad) as previously described (Nakano et al., 2017; Sato et al., 2014). *IFNB1* mRNA levels were quantified using TaqMan primer/probe sets from Thermo Fisher Scientific (#Hs01077958_s1), and primer/probe sets for *GAPDH* (NM_002046.3) served as control.

Flow Cytometry, Hematometry, and Cell Sorting

Flow cytometry was performed with FACSCanto II, FACSCalibur and FACSJazz (BD Biosciences) as previously described (Nie et al., 2009; Sato et al., 2010; Sato et al., 2012; Sato et al., 2013; Sato et al., 2014), and the obtained data were analyzed with CellQuest (BD Biosciences), FACSDiva (BD Biosciences) and FlowJo (Tree Star, Inc.) softwares. The antibodies used for flow cytometry are listed above. Hematometry was performed with a Celltac α MEK-6450 (Nihon Kohden Co.) as previously described (Nie et al., 2009; Sato et al., 2010; Sato et al., 2012; Sato et al., 2013; Sato et al., 2014). Splenic human $CD4^+$ T cells ($CD45^+CD3^+CD8^-$ cells) were isolated by using FACSJazz (BD Biosciences) as previously described (Nakano et al., 2017), and the purity was >99%.

Global Transcriptome Analysis

RNA sequencing (RNA-seq) analysis was conducted in Medical and Biological Laboratories, Co. (Nagoya, Japan). The raw sequence data (.fastq files) were mapped to the human reference genome (NCBI hg19) by Bowtie2 version 2.2.5 (Langmead and Salzberg, 2012), followed by spliced junction detection by Tophat2 version 2.1.0 (Trapnell et al., 2009). Several R (versions 3.2.3) and Bioconductor packages were used to further process the gene expression data. Read count data for each sample were extracted by package 'Rsubread' (Liao et al., 2013). The obtained raw read count data were then normalized by a method defined in package 'TCC' (Sun et al., 2013), which implements iterative DESeq2 normalization defined in package 'DESeq2' (Love et al., 2014). The normalized read count data were classified into three groups, namely, HIV-1 uninfected (mock as control), HIV-1-infected and pegIFN-treated. The expression data were analyzed to detect differentially expressed genes by package 'DESeq2' (Love et al., 2014). Top-ranked genes were selected as differentially expressed genes (DEGs) with the following threshold values: false discovery rate (FDR) less than 0.005 calculated by the Benjamini-Hochberg method (Benjamini and Hochberg, 1995); and more than twice up-regulated or less than half downregulated normalized gene expressions compared with the control. Among the top-ranked genes, low expression genes (threshold value = 1.0) were removed (see Figure 5A, Tables S2 and S4). DEGs were then used to obtain enriched biological functions by a conventional gene set enrichment analysis by using package 'clusterProfiler' (Yu et al., 2012). DEGs were also used to obtain associated pathways by applying Reactome Enrichment Pathway Analysis [package 'ReactomePA' (Yu and He, 2016)]. Associated pathways were selected with the default parameter setting: *P* value cut-off 0.05 and *Q* value cut-off 0.2 (see Tables S3 and S5). Finally, a distance matrix was calculated from the expression data for DEGs based on the correlation distance (Eisen et al., 1998), and the distance matrix was converted by the Z-transformation defined in package 'gplots' to visualize the result with a heatmap (Figure 5C).

Treatment with PegIFN and IFN-1ant

PegIFN (120 ng per mouse) (Pegasys, Chugai Pharmaceutical co.) was subcutaneously injected into humanized mice. PegIFN-treated mice were euthanized and sacrificed at 1 week post-treatment, and the human MNCs in PB and spleen were collected as

previously described (Nie et al., 2009; Sato et al., 2010; Sato et al., 2012; Sato et al., 2013; Sato et al., 2014). IFN-1ant, an antagonist specifically blocking the human IFN-α receptor (Levin et al., 2014) (2 μg per mouse per day), was intramuscularly inoculated into humanized mice.

Mathematical Modeling

To quantitatively assess the effect of Vpu on viral spread *in vivo*, we used the following previously developed model (Ikeda et al., 2016):

$$\frac{dT(t)}{dt} = -\beta T(t)V(t), \quad \text{(Equation 1)}$$

$$\frac{dV(t)}{dt} = rT(t)V(t) - \delta V(t), \quad \text{(Equation 2)}$$

where $T(t)$ and $V(t)$ are the densities of target cells and virus particles, and applied the model to time course data of the number of $CD4^+$ T cells (i.e., the target cells) per ml of PB and the viral RNA load (i.e., the virus particles) per ml of plasma of infected humanized mice. As described in our previous study (Ikeda et al., 2016), we performed Bayesian estimation using Markov Chain Monte Carlo (MCMC) sampling, and estimated distributions of the parameters. Estimated parameters are summarized in Table S1.

QUANTIFICATION AND STATISTICAL ANALYSIS

Unless otherwise stated, data analyses were performed using GraphPad Prism software. The data are presented as averages ± SEM. Statistically significant differences were determined by Mann-Whitney U test or paired *t* test. To determine statistically significant correlations, the Spearman rank correlation test was applied. Statistical details can be found directly in the figures or in the corresponding figure legends.

DATA AND SOFTWARE AVAILABILITY

The transcriptome data of the splenic human $CD4^+$ T cells of HIV-1-infected mice (n = 2), pegIFN-treated mice (n = 2) and mock-infected mice (n = 2) are deposited under the accession number GEO: GSE94776.